Transcriptome and proteome profiling reveals complex adaptations of *Candida parapsilosis* cells assimilating hydroxyaromatic carbon sources

Andrea Cillingová[1], Renáta Tóth[2,3], Anna Mojáková[1], Igor Zeman[1], Romana Vrzoňová[1], Barbara Siváková[4], Peter Baráth[4], Martina Neboháčová[1], Zuzana Klepcová[1], Filip Brázdovič[1], Hana Lichancová[1], Viktória Hodorová[1], Broňa Brejová[5], Tomáš Vinař[6], Ľubomír Tomáška[7], Atilla Gácser[2,3], Toni Gabaldón[8,9,10], Jozef Nosek[1*]

[1] Department of Biochemistry, Faculty of Natural Sciences, Comenius University in Bratislava, Ilkovičova 6, 842 15 Bratislava, Slovakia

[2] HCEMM-USZ Department of Microbiology, University of Szeged, Közép fasor 52, H-6726 Szeged, Hungary

[3] MTA-SZTE Lendület Mycobiome Research Group, University of Szeged, Szeged, Hungary

[4] Institute of Chemistry, Slovak Academy of Sciences, Dúbravská cesta 9, 845 38 Bratislava, Slovakia

[5] Department of Computer Science, Faculty of Mathematics, Physics and Informatics, Comenius University in Bratislava, Bratislava, Slovakia

[6] Department of Applied Informatics, Faculty of Mathematics, Physics and Informatics, Comenius University in Bratislava, Bratislava, Slovakia

[7] Department of Genetics, Faculty of Natural Sciences, Comenius University in Bratislava, Ilkovičova 6, 842 15 Bratislava, Slovakia

[8] Institute for Research in Biomedicine (IRB), The Barcelona Institute of Science and Technology, Baldiri Reixac, 10, 08028 Barcelona, Spain

[9] Barcelona Supercomputing Centre (BSC-CNS). Jordi Girona, 29. 08034. Barcelona, Spain

[10] Catalan Institution for Research and Advanced Studies (ICREA), Barcelona, Spain

* Corresponding author

E-mail: jozef.nosek@uniba.sk (JN)

Short title: Metabolic adaptation of *C. parapsilosis* to hydroxyaromatic substrates

Abstract

Many fungal species utilize hydroxyderivatives of benzene and benzoic acid as carbon sources. The yeast *Candida parapsilosis* metabolizes these compounds via the 3-oxoadipate and gentisate pathways, whose components are encoded by two metabolic gene clusters. In this study, we determine the chromosome level assembly of the *C. parapsilosis* strain CLIB214 and use it for transcriptomic and proteomic investigation of cells cultivated on hydroxyaromatic substrates. We demonstrate that the genes coding for enzymes and plasma membrane transporters involved in the 3-oxoadipate and gentisate pathways are highly upregulated and their expression is controlled in a substrate-specific manner. However, regulatory proteins involved in this process are not known. Using the knockout mutants, we show that putative transcriptional factors encoded by the genes *OTF1* and *GTF1* located within these gene clusters function as transcriptional activators of the 3-oxoadipate and gentisate pathway, respectively. We also show that the activation of both pathways is accompanied by upregulation of genes for the enzymes involved in β-oxidation of fatty acids, glyoxylate cycle, amino acid metabolism, and peroxisome biogenesis. Transcriptome and proteome profiles of the cells grown on 4-hydroxybenzoate and 3-hydroxybenzoate, which are metabolized via the 3-oxoadipate and gentisate pathway, respectively, reflect their different connection to central metabolism. Yet we find that the expression profiles differ also in the cells assimilating 4-hydroxybenzoate and hydroquinone, which are both metabolized in the same pathway. This finding is consistent with the phenotype of the Otf1p-lacking mutant, which exhibits impaired growth on hydroxybenzoates, but still utilizes hydroxybenzenes, thus indicating that additional, yet unidentified transcription factor could be involved in the 3-oxoadipate pathway regulation. Moreover, we propose that bicarbonate ions resulting from decarboxylation of hydroxybenzoates also contribute to differences in the cell responses to hydroxybenzoates and hydroxybenzenes. Finally, our phylogenetic analysis highlights evolutionary paths leading to metabolic adaptations of yeast cells assimilating hydroxyaromatic substrates.

Author summary

Benzene and its derivatives are simple aromatic compounds representing key substances for the chemical industry. While benzene itself is toxic and carcinogenic, benzoic acid is commonly used in the food industry and some of its derivatives are used in pharmacology (aspirin) or cosmetics (parabens). The benzene ring of aromatic molecules is relatively stable, but many microorganisms including yeasts break it enzymatically and, in a series of biochemical reactions, utilize resulting metabolites as carbon sources. Understanding the genetic basis of corresponding metabolic pathways and their regulation opens a venue for applications in biotechnology and bioremediation of polluted environments. Here we investigate the yeast *Candida parapsilosis* which assimilates various hydroxybenzenes and hydroxybenzoates via the 3-oxoadipate and gentisate pathways. We show that the genes coding for the substrate transporters and enzymes involved in both pathways are co-expressed and regulated by the transcriptional activators Otf1p and Gtf1p, respectively. Our results also reveal the connections of both pathways to central metabolism and organelle biogenesis and provide an insight into evolution of metabolism of hydroxyaromatic compounds.

Introduction

Metabolic gene clusters (MGCs) are composed of co-localized genes, whose products participate in the same metabolic pathway. In most cases, their functions are linked to the production of secondary metabolites or the assimilation of unconventional substrates. Such biochemical pathways are usually nonessential, but in specific circumstances they may provide a growth benefit for the host organism. In general, MGCs encode the enzymes catalyzing reactions in a biochemical pathway, membrane transporters for substrates or metabolites, as well as transcription factors that control the expression of corresponding genes. Gene clustering thus generates functional genetic modules whose co-regulated expression facilitates rapid adaptation of cellular metabolism to environmental changes (1,2). The occurrence of MGCs in eukaryotic genomes was originally considered to be rare. However, bioinformatic analyses of a constantly increasing number of sequenced genomes show that the gene clusters are their typical feature, especially in case of fungal and plant genomes (3-5). The formation of MGCs also facilitates their transmission via horizontal gene transfer, thus contributing to metabolic diversity of fungal species and their ecological adaptation (6). Investigations of MGCs provide a venue for elucidating their evolutionary origin, genetic organization, and expression, as well as the coordination of the corresponding biochemical pathways with the central cellular metabolism.

Previously, we identified and characterized several genes from the pathogenic yeast *Candida parapsilosis* arranged in two MGCs, which are conserved in the genomes of yeast species from the 'CUG-Ser1' clade of the subphylum Saccharomycotina (7-12). These MGCs code for enzymes of the gentisate (GP) and 3-oxoadipate (3-OAP) pathways that are involved in catabolic degradation of a broad spectrum of hydroxyderivatives of benzene and benzoic acid. While 3-hydroxybenzoate and gentisate (2,5-dihydroxybenzoate) are metabolized via the GP, 4-hydroxybenzoate, 2,4-dihydroxybenzoate, protocatechuate (3,4-dihydroxybenzoate), hydroquinone, and resorcinol are degraded via the hydroxyhydroquinone (HHQ) branch of the 3-OAP (13,14). The resulting products of both biochemical pathways (i.e. fumarate and pyruvate in the GP; succinate and acetyl-CoA in the 3-OAP) can be channeled into tricarboxylic acid (TCA) cycle operating in mitochondria. Interconnection of both pathways with these organelles is mediated by metabolite carriers in the inner mitochondrial membrane (i.e. Sfc1p, Leu5p, Yhm2p, and Mpc1p). Moreover, the enzymes catalyzing the last two steps of the 3-OAP (i.e. 3-oxoadipate:succinyl-CoA transferase (Osc1p) and 3-oxoadipyl-CoA thiolase

(Oct1p)) are imported into mitochondria (9,11). In addition, we have previously identified a family of genes coding for the plasma membrane transporters for hydroxybenzoates (10). Moreover, while both pathways are repressed in cells assimilating glucose, corresponding genes are highly induced during cultivation on media containing a hydroxyaromatic substrate as a sole carbon source (7,9-11). Although the transcriptional factors involved in this regulation have not yet been identified, both MGCs contain a gene for uncharacterized zinc cluster transcription factor representing a candidate transcriptional activator of the corresponding pathway.

In this study, we investigate the regulation of the 3-OAP and GP as well as the coordination of both pathways with central metabolism and organelle biogenesis. Using the analysis of transcriptomic and proteomic profiles of *C. parapsilosis* cells assimilating hydroxyaromatic compounds we show that the induction of both pathways is accompanied by the upregulation of genes whose products are involved in β-oxidation of fatty acids (FA), glyoxylate cycle, metabolism of amino acids, and the biogenesis of peroxisomes. Our results also highlight the differences between the metabolism of hydroxybenzoates and hydroxybenzenes. Moreover, we demonstrate experimentally that putative transcription factors named Gtf1p and Otf1p function as transcriptional activators of the GP and 3-OAP genes, respectively. Their phylogenetic analysis shed additional insight into the evolution of both biochemical pathways.

Results and Discussion

Gene expression landscape of *C. parapsilosis* cells assimilating hydroxyaromatic carbon sources. Several studies have demonstrated that *C. parapsilosis* assimilates a broad spectrum of hydroxyderivatives of benzene and benzoic acid via the GP and 3-OAP (7,13). To investigate the regulation of both pathways we analyzed *C. parapsilosis* cells grown in media containing hydroxyaromatic compounds degraded either via the 3-OAP or GP. The gene expression analysis was performed in the strain CLIB214 (CBS604), which is together with derived mutants commonly used in experimental studies (e.g. 15-18). This strain was originally isolated from a patient with tropical diarrhea in Puerto Rico (19) and it represents the type strain of *C. parapsilosis*. Although a genome sequence survey of CLIB214 was carried out in 2005 by Sanger sequencing (20), the complete genome sequence of this strain was not available. Here, we determined the chromosome level genome assembly of the CLIB214 strain by combining Oxford Nanopore and Illumina sequencing technologies and used it for analyses of cells utilizing hydroxyaromatic substrates (see below). The resulting CLIB214 assembly has a total length of 13.0 Mbp and consists of 8 nuclear chromosomes corresponding to the electrophoretic karyotype determined by PFGE (**Fig 1**). Alignments with the reference genome sequence of the strain CDC317 (21) cover 99.5% of the assembly and have a 99.9% identity. Compared to the CDC317 assembly, there is a single large-scale translocation between chromosomes 4 and 5 (CDC317 contigs HE605208.1 and HE605204.1). Annotation of the nuclear chromosomes contains 5,856 predicted protein-coding genes; 5,797 of them overlap with protein coding genes mapped from the CDC317 strain. The six genes coding for the GP components (i.e. *MNX2, HBT1*, *GDX1*, *FPH1*, *GFA1, GTF1*) are localized in a single MGC which is present in the subtelomeric region of chromosome 6. The 3-OAP components are encoded by a cluster comprising four genes (i.e. *FRD1*, *HDX1*, *OSC1, OTF1*) located on chromosome 5, as well as by several additional loci on chromosomes 1 and 2 (**Fig 1)**.

Fig 1. Nuclear genome organization of the *C. parapsilosis* strain CLIB214.

(A) Chromosomal contigs of *C. parapsilosis* CLIB214. The colouring is based on alignments with the nuclear contigs of the reference genome sequence (CDC317) (see Materials and Methods for details). (B) Electrophoretic karyotype of CLIB214. DNA samples prepared in agarose blocks were separated

by PFGE at three different conditions (I, II, and III) as described in Materials and Methods. The bands corresponding to the chromosome containing an rDNA array (0.98 Mbp) and the linear mitochondrial DNA (32.8 kbp) are indicated by one and two asterisks, respectively. (C) Organization of the GP and 3-OAP gene clusters. The genes coding for the transcription activators Gtf1p and Otf1p investigated in this study are shown in black.

Next, we used the CLIB214 genome assembly as a reference for transcriptomic and proteomic experiments to investigate the activation of genes involved in the 3-OAP and GP and their links to central cellular metabolism and organelle biogenesis. In these experiments, we compared CLIB214 cells assimilating 4-hydroxybenzoate, hydroquinone (both metabolized via the 3-OAP) and 3-hydroxybenzoate (metabolized via the GP), with those utilizing galactose as a control carbon source. By RNA-Seq analysis, we identified 270, 435, and 365 genes upregulated more than four-fold in cells cultivated in media containing 3-hydroxybenzoate, 4-hydroxybenzoate, and hydroquinone, respectively, compared to control cells grown on galactose (**Fig 2**, **S1 Table)**.

Fig 2. Differentially expressed genes identified by RNA-Seq analysis.

The Venn diagrams show numbers of upregulated (log_2 fold change ≥ 2; p ≤ 0.05; (A)) or downregulated (log_2 fold change ≤ -2; p ≤ 0.05; (B)) genes in CLIB214 cells assimilating 3-hydroxybenzoate, 4-hydroxybenzoate or hydroquinone compared to galactose. The results are based on the lists of differentially expressed genes (**S1 Table**). The diagrams were drawn with a web tool (http://bioinformatics.psb.ugent.be/webtools/Venn/).

In line with our previous reports (7,9,10), the RNA-Seq analysis showed that the genes encoding the enzymes catalyzing reactions in each pathway as well as the plasma membrane carriers facilitating the transport of hydroxybenzoates (**Fig 3A**) are co-regulated in a substrate-specific manner. Specifically, the GP cluster genes are highly upregulated (i.e. between 267- (*GFA1*) and 3,061-fold (*HBT1*)) in the cells assimilating 3-hydroxybenzoate, which is metabolized via the GP. These genes exhibit only minor

177 changes in media containing 4-hydroxybenzoate, except for *GTF1* and *HBT1* showing about 12.6- and
178 4.7-fold induction on this substrate, respectively (**Fig 3B**, **S1 Table**). The genes for the 3-OAP enzymes
179 and two plasma membrane transporters (*HBT2* and its paralog *HBT3*) are highly upregulated on both
180 4-hydroxybenzoate (i.e. between 46.5- (*OSC1*) to 1,090-fold (*HBT2*)) and hydroquinone (i.e. between
181 8.1- (*HBT3*) and 208-fold (*HDX1*)). Expression of these genes changes only slightly on the GP
182 substrate, except *MNX1* which exhibits about 19-fold increase (**Fig 3B**, **S1 Table**).
183
184
185 **Fig 3. The 3-OAP and GP are induced in *C. parapsilosis* cells assimilating hydroxyaromatic**
186 **compounds.**
187 (A) The simplified schemes depicting the enzymes and hydroxybenzoate transporters involved in the
188 3-OAP and GP in *C. parapsilosis*. (B) Differential expression of selected *C. parapsilosis* genes involved
189 in the metabolism of hydroxyaromatic compounds. The expression was analyzed in CLIB214 cells
190 grown to OD_{600} ~ 1 in synthetic media containing 3-hydroxybenzoate, 4-hydroxybenzoate or
191 hydroquinone as a sole carbon source compared to the cells cultivated in medium with galactose (i.e.
192 S3OH vs. SGal, S4OH vs. SGal, SHyd vs. SGal) or 4-hydroxybenzoate (S3OH vs. S4OH, SHyd vs.
193 S4OH). Analysis of the mutants Δ*gtf1*/Δ*gtf1* and Δ*otf1*/Δ*otf1* is based on the comparison to the parental
194 strain CPL2H1 (Δ*gtf1*/Δ*gtf1* vs. CPL2H1 and Δ*otf1*/Δ*otf1* vs. CPL2H1) grown in an SMix15 medium
195 containing three hydroxyaromatic carbon sources (i.e. 3-hydroxybenzoate, 4-hydroxybenzoate, and
196 hydroquinone). The $\log_2$ fold change values are shown (**S1 Table** and **S2 Table**). Note that the values
197 that are not statistically significant (i.e. $p > 0.05$) are shown in parentheses. (C) LC-MS/MS analysis of
198 protein extracts from *C. parapsilosis* CLIB214. The cells were pre-cultivated overnight in an S3OH
199 medium, inoculated to SGal, S3OH, S4OH, and SHyd media, and grown to ~ 10^7 cells/ml. Soluble
200 proteins were extracted and analyzed by LC-MS/MS. Log2 values of mean LFQ intensity ratios are
201 shown (**S3 Table**). For proteins that were not identified on all carbon sources the LFQ values imputed
202 from a normal distribution were used in the calculation (indicated in parentheses).
203
204
205 Next, we analyzed the proteins in the cellular extracts prepared from the CLIB214 cultures by LC-
206 MS/MS. In total, we identified 1451 proteins, of which 1176 had significantly different relative abundance

(based on LFQ values) as evaluated by ANOVA test. The comparison of the 3-OAP and GP related proteins identified in the cells assimilating hydroxyaromatic substrates with those utilizing galactose shows a pattern similar to the RNA-Seq results, i.e. the 3-OAP enzymes are highly enriched on both 4-hydroxybenzoate and hydroquinone, and the GP enzymes are enriched on 3-hydroxybenzoate (**Fig 3C**, **S3 Table**). However, we did not identify several proteins (i.e. Hbt3p, Hbt4p, Gtf1p, Otf1p). We presume that this is caused by overall low abundance of these polypeptides in the cells or their depletion from the prepared extracts due to insolubility or subcellular localization.

The MGCs contain yet uncharacterized genes *FRD1* and *GFA1* which are highly induced on hydroxyaromatic substrates and appear to be co-regulated with the genes for the 3-OAP or GP enzymes, respectively. This indicates that their products could participate in the metabolism of hydroxyaromatic substrates. Based on the expression profiles and identified protein domains, we hypothesize that *FRD1* (flavin reductase 1; *CANPARB_p44520-A* (*CPAR2_406430* in CDC317)) and *GFA1* (glutathione-dependent formaldehyde-activating enzyme 1; *CANPARB_p50380-A* (*CPAR2_704360* in CDC317)) code for maleylacetate reductase and glutathione-dependent maleylpyruvate isomerase involved in the 3-OAP and GP, respectively. Moreover, the transcriptome analysis also revealed that two neighboring open reading frames (ORFs) *CANPARB_p44920-A* and *CANPARB_p44910-A* also belong to highly upregulated genes (i.e. 83- and 103-fold, respectively) in CLIB214 cells assimilating 3-hydroxybenzoate compared to galactose. These ORFs are not annotated in the reference genome (CDC317), although their sequences are identical in both strains. The deduced amino acid sequences of CANPARB_p44920-A and CANPARB_p44910-A are highly similar to the N- and C-terminal half, respectively, of bacterial proteins from the amidohydrolase superfamily, which includes 2-amino-3-carboxymuconate-6-semialdehyde decarboxylase (ACMSD), orsellinate decarboxylase (OrsB), 6-methylsalicylate decarboxylase (YanB), and salicylate decarboxylase involved in metabolism of various hydroxyaromatic compounds (**S1 Fig**, see below for a more detailed discussion).

Metabolic pathways activated in cells assimilating hydroxyaromatic compounds. Gene ontology (GO) analysis revealed that the lists of upregulated genes in the RNA-Seq experiment are enriched for categories annotated as oxidoreductase (13.7%), hydrolase (10.7%), transferase (9.0%), transporter

(8.2%), DNA- (6.1%), and protein-binding (5.8%) activities. The KEGG mapper analysis identified 163 upregulated genes coding for enzymes involved in metabolic pathways (**Fig 4**, **S2 Fig**). A large proportion of these enzymes are involved in FA metabolism (22) including those involved in β-oxidation and lipases involved in mobilization of FAs from mono- and triglycerides (MAG and TAG lipases) and (lyso)phospholipids (phospholipases B/A2). The supposedly increased level of hydrogen peroxide in peroxisomes is accompanied by overexpression of the genes for catalases, superoxide dismutase, and glutathione-*S*-transferases. Although the localization of these proteins in peroxisomes was not tested experimentally, it can be supposed that the catalase isoenzymes play a protective role in β-oxidation (23). Furthermore, the β-oxidation cycle is provided by acyl-CoA by the action of fatty acid-CoA synthetases (FAAs) that constitute an unusually large family of isoenzymes in *C. parapsilosis*. In *Saccharomyces cerevisiae,* there are four FAAs with various roles in FA metabolism, transport, acylation of proteins, vesicular transport, and transcription regulation (24). *C. albicans*, *C. auris*, *C. dubliniensis*, and *C. glabrata* contain up to five FAAs, whereas *C. parapsilosis* contains twelve FAA-encoding genes. Nine of them are highly upregulated ($\log_2$ fold change > 2) on at least one substrate and five on all three tested hydroxyaromatic carbon sources (**S3 Fig**). Acetyl-CoA resulting from β-oxidation is feeding downstream metabolic processes including glyoxylate cycle. Indeed, the genes for citrate synthase (*CIT1*), isocitrate lyase (*ICL1*), and malate synthase (*MLS1*) are upregulated and so CoA can be provided back to β-oxidation (25). The gene encoding a peroxisomal coenzyme A diphosphatase (*PCD1*) regenerating CoA within peroxisomes (26) is also upregulated. In addition, the genes encoding enzymes involved in carnitine shuttle, such as *CAT2* encoding a homolog of a major form of carnitine acetyltransferase with dual localization to mitochondria and peroxisomes, are upregulated supplying a shuttle of acetyl units between these organelles (27). Finally, the genes for numerous enzymes involved in metabolism of amino acids, vitamins, purines, and pyrimidines are also overexpressed thus contributing to the metabolic needs of the cells utilizing hydroxyaromatic substrates (**S2 Fig**). In many cases, the gene expression profiles based on the RNA-Seq experiment more or less correspond to those obtained by the LC-MS/MS analysis. However, there are several notable differences. In particular, the genes coding for the three glyoxylate cycle enzymes, namely citrate synthase (Cit1p), isocitrate lyase (Icl1p), and malate synthase (Mls1p) exhibit upregulated transcription (log2 fold change ≥ 2) both on 3-hydroxybenzoate and 4-hydroxybenzoate, yet the LC-MS/MS analysis indicates a slight decrease of the corresponding proteins on the former substrate. Discordances

between mRNA and protein levels are usually caused by posttranscriptional regulation of protein synthesis and/or degradation (28,29). The observed differences in transcriptome and proteome profiles imply that the interconnection of final products of the GP and 3-OAP with the intermediate metabolism differs. The last step of the GP occurs in cytosol (9) producing pyruvate and fumarate. The former could be carboxylated to oxaloacetate (30) thus supplying the substrate for sugar synthesis in the same compartment. On the other hand, the 3-OAP producing succinate and acetyl-CoA in mitochondria (11) needs the peroxisomal glyoxylate cycle to convert the latter C2 unit to C4 to supply the gluconeogenesis with a C4 substrate (31).

Fig 4. Major metabolic pathways upregulated in the cells utilizing 3-hydroxybenzoate, 4-hydroxybenzoate or hydroquinone as a sole carbon source.
(A,C) The glyoxylate cycle, β-oxidation, and (B,D) modified β-oxidation pathway (32) are depicted in a simplified form. The expression profiles obtained by the RNA-Seq (A,B; **S1 Table**) and LC-MS/MS analyses (C,D; **S3 Table**) are shown. The three squares illustrate the gene expression changes on different hydroxyaromatic substrates compared to galactose as indicated in the legend in the upper left corner on panels (A) and (C). Only the genes whose transcription was overexpressed on at least one hydroxyaromatic substrate are shown. Note that not all enzymes listed in **S2 Fig** and **S4 Fig** are shown on the scheme.

Catabolism of hydroxyaromatic compounds leads to upregulation of genes involved in the biogenesis and metabolism of peroxisomes. Previously, we reported that catabolism of hydroxyaromatic compounds is linked to mitochondria (9). Here we show that peroxisomes also play a role in cellular response to these substrates. These organelles are highly dynamic and tightly regulated by processes of *de novo* formation, division, and autophagic degradation. In yeast cells, their number depends on the utilized carbon source (33). The fact that boosting FA catabolism is accompanied by proliferation of peroxisomes in *C. parapsilosis* is underlined not only by upregulation of genes for metabolic enzymes, but also those involved in peroxisome biogenesis (**Fig 5A**; **S4 Fig**) including Pex11p crucial for peroxisome proliferation (34,35), Pex3p and Pex19p essential for the formation of

297 peroxisomal membrane (36), receptors Pex5p and Pex7p, and other components of matrix protein
298 importomer, namely Pex1p, Pex2p, Pex4p, Pex8p, Pex10p, Pex12p-Pex14p, and Pex17p (37). In
299 addition, the gene coding for inheritance protein Inp1p which secures a balanced distribution of
300 peroxisomes between mother and daughter cells is also upregulated (38). To demonstrate the presence
301 of peroxisomes in cells assimilating the 3-OAP and GP substrates, we constructed the plasmid pBP7-
302 mCherry-SKL expressing a soluble codon-optimized mCherry protein (39) tagged with peroxisomal
303 targeting signal type 1 (PTS1) serine–lysine–leucine (SKL) at its C-terminus. The plasmid pBP7-
304 mCherry expressing an unmodified marker was used as a control. Both plasmids were introduced into
305 *C. parapsilosis* CDU1 cells and the transformants were grown in synthetic media containing galactose.
306 Cells containing pBP7-mCherry-SKL were also cultivated in synthetic media containing 3-
307 hydroxybenzoate or 4-hydroxybenzoate as a sole carbon source. Examination of the transformants by
308 fluorescence microscopy showed the presence of multiple bright foci in the cells expressing mCherry-
309 SKL protein. The control cells carrying the pBP7-mCherry plasmid show cytosolic localization of the
310 marker (**Fig 5B**). This result indicates that cells utilizing hydroxybenzoate substrates metabolized via
311 the 3-OAP or GP contain multiple peroxisomes, although their number and size in the cells grown on
312 hydroxybenzoate substrates and galactose do not seem to be substantially different.
313
314
315 **Fig 5. Peroxisomes are involved in the catabolism of hydroxyaromatic compounds.**
316 (A) The Venn diagram illustrating numbers of upregulated genes involved in the biogenesis and
317 metabolism of peroxisomes identified by RNA-Seq analysis of CLIB214 cells assimilating 3-
318 hydroxybenzoate, 4-hydroxybenzoate or hydroquinone compared to galactose. The upregulated genes
319 ($\log_2$ fold change ≥ 2; $p \leq 0.05$) classified into categories 'peroxisome', 'peroxisomal matrix',
320 'peroxisomal membrane' or 'peroxisomal importomer complex' (based on the GO subcellular
321 component analysis; http://www.candidagenome.org) were selected from the lists of differentially
322 expressed genes (**S1 Table; S4 Fig**). The diagram was drawn with a web tool
323 (http://bioinformatics.psb.ugent.be/webtools/Venn/). (B) *C. parapsilosis* CDU1 cells expressing
324 cytosolic (mCherry) and peroxisomal (mCherry-SKL) versions of the marker protein. The cells were
325 transformed with pBP7-mCherry or pBP7-mCherry-SKL plasmids and the transformants were cultivated
326 on a synthetic medium with galactose, 3-hydroxybenzoate or 4-hydroxybenzoate at 28 °C.

***C. parapsilosis* response to hydroxybenzenes and hydroxybenzoates.** The size and morphology of the *C. parapsilosis* colonies grown in synthetic media indicate that the cells respond differently to assimilated hydroxyaromatic substrates (**Fig 6A**). The RNA-Seq analysis of the cells utilizing 3-hydroxybenzoate, 4-hydroxybenzoate or hydroquinone show that although there is a group of ninety nine genes upregulated on any of the three carbon sources, many genes are selectively induced only on a single substrate (**Fig 2A**). As 3-hydroxybenzoate and 4-hydroxybenzoate are catabolized by distinct biochemical pathways producing different metabolites (i.e. acetyl-CoA and succinate in the 3-OAP, fumarate and pyruvate in the GP), the differences in transcription profiles of cells utilizing these substrates may reflect, at least in part, different links of these pathways to central metabolism. However, 4-hydroxybenzoate and hydroquinone are degraded in the same pathway (i.e. 3-OAP), yet only about a half of the upregulated genes are induced on both substrates and the difference in the lists of downregulated genes on these substrates is even greater (**Fig 2**). In the 3-OAP, hydroxybenzoates are decarboxylated to hydroxybenzenes (i.e. 4-hydroxybenzoate to hydroquinone; 2,4-dihydroxybenzoate and protocatechuate to hydroxyhydroquinone). The decarboxylation step is catalyzed by the monooxygenase Mnx1p which has broad substrate specificity (40,41). This reaction releases a molecule of carbon dioxide, which can be readily converted by carbonic anhydrase to a bicarbonate anion (HCO_3^-). To monitor the formation of bicarbonate anions we cultivated CLIB214 cells in synthetic media containing various carbon sources and a pH indicator (bromothymol blue, p*K*a=7). We observed dramatic pH changes in the cultures grown on hydroxybenzenes compared to those assimilating hydroxybenzoates. As judged from the color of the pH indicator observed at later cultivation stages (> 12 hours), the media were acidified when the cells assimilated hydroquinone or resorcinol, which is also typical for sugar utilization (42). In contrast, the cells utilizing hydroxybenzoates (i.e. 4-hydroxybenzoate, protocatechuate, 3-hydroxybenzoate, gentisate) alkalinized the medium pointing to a buffering effect of generated bicarbonate anions (**Fig 6B**). As these ions have a role in intracellular signaling (via activation of adenylyl cyclase) and the control of metabolism (43), our results indicate that assimilation of hydroxyaromatic substrates is accompanied by a complex cellular response which is dependent on particular carbon source.

Fig 6. Colony morphology and pH changes in cultivation media.

(A) Morphology of CLIB214 colonies grown in synthetic media differing by the carbon source. The cells were pre-grown in a complex medium (YPD) for 24 h at 28°C, washed with water, resuspended to ~10^7 cells/ml and 40 µl aliquots were spotted onto Petri plates containing synthetic media with indicated carbon source. The plates were incubated for 30 days at 28°C. (B) CLIB214 cells assimilating hydroxyaromatic substrates alter the pH of cultivation media. The cells were cultivated in liquid synthetic media containing indicated carbon source and bromothymol blue as pH indicator (see Materials and Methods for details). The cultures were grown for up to 60 hours at 28 °C. The cells were removed by centrifugation and the cultivation media as well as the cell-free controls were transferred into wells of a 96-well plate and photographed.

***OTF1* and *GTF1* code for $Zn(II)_2Cys_6$ transcription activators involved in the control of the 3-OAP and GP genes, respectively.** As mentioned above the 3-OAP and GP gene clusters contain the genes *OTF1* and *GTF1*, respectively, coding for putative transcription factors. The predicted proteins are 963 and 741 amino acids long, respectively, and contain Gal4-like $Zn(II)_2Cys_6$ zinc cluster DNA-binding and fungal transcription factor domains as well as putative nuclear localization signals (NLS) indicating their import into the cell nucleus (**S5 Fig**). As the orthologs of these genes are conserved in several species belonging to the 'CUG-Ser1' clade (see below) which assimilate hydroxyaromatic compounds (7-9) we hypothesized that *OTF1* (3-oxoadipate pathway transcription factor 1; *CANPARB_p44550-A* (*CPAR2_406460* in CDC317)) and *GTF1* (gentisate pathway transcription factor 1; *CANPARB_p50390-A* (*CPAR2_704370* in CDC317)) control the expression of corresponding MGC.

First, we confirmed that Otf1p and Gtf1p are targeted into the cell nucleus. We prepared the plasmid constructs expressing these proteins tagged with yEGFP3 at their N-termini (i.e. yEGFP3-Otf1p, yEGFP3-Gtf1p) in *C. parapsilosis* SR23 $met1^-$ cells. Examination by fluorescence microscopy showed that both proteins co-localize with DAPI-stained nuclear DNA. Moreover, yEGFP3-Gtf1p appears to be concentrated in distinct foci pointing to its specific subnuclear localization. We presume that it associates with the promoters of the GP cluster genes present in the subtelomeric region of chromosome 6 (**Fig 7**).

Fig 7. Transcription factors Otf1p and Gtf1 tagged with yEGFP3 at their N-termini localize in the cell nuclei.

C. parapsilosis SR23 met1^{-} cells transformed with pPK6, pPK6-OTF1 or pPK6-GTF1 plasmids were grown overnight in an SGal medium. The cells were washed with water and DNA in cells was stained with DAPI.

To demonstrate that Otf1p and Gtf1p are involved in the transcriptional control of the 3-OAP and GP, respectively, we constructed knockout strains lacking both alleles of *OTF1* or *GTF1* and tested their ability to utilize different hydroxybenzenes and hydroxybenzoates as a sole carbon source. We found that the Δ*otf1*/Δ*otf1* mutant exhibits a growth defect on several substrates metabolized via the 3-OAP. While its growth is impaired in media containing hydroxybenzoates (i.e. 4-hydroxybenzoate, 2,4-dihydroxybenzoate, 3,4-dihydroxybenzoate), we did not observe a growth defect in media containing hydroxybenzenes (resorcinol, hydroquinone). On the other hand, the Δ*gtf1*/Δ*gtf1* mutant is unable to grow in media containing 3-hydroxybenzoate or gentisate, which are degraded via the GP (**Fig 8**). The phenotypes of both mutants indicate that Otf1p and Gtf1p are involved in the control of the 3-OAP and GP, respectively.

Fig 8. *C. parapsilosis* mutants Δ*otf1*/Δ*otf1* and Δ*gtf1*/Δ*gtf1* exhibit impaired growth on hydroxyaromatic substrates.

Indicated strains were pre-grown overnight in a complex medium (YPD) at 28 °C, washed with water and resuspended to ~6×10^6 cells/ml. Serial fivefold dilutions were then spotted on solid synthetic media containing indicated carbon sources. The plates were incubated for 4 days at 28 °C.

To investigate the role of Otf1p and Gtf1p in the control of the 3-OAP and GP genes, respectively, we compared the transcriptomic profiles of the knockout mutants with the parental strain CPL2H1 cultivated

in synthetic medium containing a mixture of hydroxyaromatic carbon sources (i.e. 3-hydroxybenzoate, 4-hydroxybenzoate, and hydroquinone) metabolized via the GP or 3-OAP. The RNA-Seq experiment demonstrated that expression of the genes present in the GP gene cluster is substantially decreased in the Δ*gtf1*/Δ*gtf1* mutant compared to the parental strain (**Fig 3, S2 Table**, **S6 Fig).** In addition, we found that the transcript(s) derived from *CANPARB_p44920-A* and *CANPARB_p44910-A* ORFs coding for a predicted amidohydrolase superfamily protein is almost absent in this mutant.

A comparison of the Δ*otf1*/Δ*otf1* mutant and CPL2H1 cells revealed more subtle differences in the expression of genes for the 3-OAP enzymes. We found that *MNX1* and *HBT2* are downregulated by 6.37- and 1.97-fold, respectively (**Fig 3**, **S2 Table**, **S6 Fig)**. As these genes code for 4-hydroxybenzoate 1-hydroxylase decarboxylating hydroxybenzoates to hydroxybenzenes (7,40,41) and a hydroxybenzoate transporter (10), their decreased expression goes in line with the observation that the Δ*otf1*/Δ*otf1* mutant has impaired growth on hydroxybenzoates (**Fig 7**). The expression of the genes *MNX3, HDX1*, *FRD1*, *OSC1*, and *OCT1* encoding remaining enzymes of the 3-OAP is also slightly decreased (i.e. by 1.45 to 1.90-fold). However, as the mutant grows on media with hydroquinone or resorcinol, we assume that expression of these genes is sufficient for utilization of both hydroxybenzenes.

Otf1p and Gtf1p recognize specific motifs in promoter sequences. As described above, the genes coding for the enzymes of the 3-OAP and GP are highly upregulated in the cells assimilating hydroxyaromatic substrates. To identify potential regulatory motifs involved in their transcriptional control, we searched corresponding promoter sequences for putative Otf1p- and Gtf1p-binding sites. Both transcription factors belong to the Gal4-like family whose members recognize sequences containing CGG triplets oriented as inverted repeats separated by a distinct number of nucleotides, although other terminal nucleotides such as GGA were also identified in the binding sites (44,45). Moreover, Otf1p is a homolog of the transcription factor *qa-1F* activating expression of the quinic acid gene cluster in *Neurospora crassa*, which recognizes a 16-mer motif GGATAATCGATTATCC (46). The search of the *MNX1* promoter sequence revealed a similar motif $GGRN_{10}WCC$ occurring at positions -1376 to -1361 and -812 to -797. We also found that this motif is present in the promoters of other genes coding for the 3-OAP enzymes (i.e. *FRD1*, *HDX1, MNX3*, *OCT1, OSC1*), hydroxybenzoate transporter

(*HBT2*) and its paralogs (*HBT3*, *HBT4*) (**S7 Fig**, **S8 Fig**) which are co-induced in the cells grown in media with 4-hydroxybenzoate or hydroquinone (**Fig 3**). Distribution of the $GGRN_{10}WCC$ motif indicates that it represents a potential binding site for the transcription factor Otf1p. To search for putative Gtf1p-binding sites, we analyzed the promoters of the GP cluster genes using the MEME tool (http://meme-suite.org; (47)) and identified a motif $TCGGN_8TCC$ (E-value = 2.7e-1) which occurs upstream of each ORF in the GP gene cluster, except for the *GTF1* gene. Alignment of the identified hits including their flanking sequences allowed us to refine the consensus sequence to a $GGAN_7TCC$ motif (**S7 Fig**, **S8 Fig**). Four putative Gtf1p-binding sites occur at positions -1111 to -1099, -428 to -416, -299 to -287, and -263 to -251 upstream of the *MNX2* coding sequence. As the first site is closer to the *HBT1* ORF (i.e. -366 to -354), we assume that it may be involved in the control of this gene. Additional sites present in the GP gene cluster occur in the intergenic region between *GDX1* and *FPH1* (i.e. -191 to -179 and -201 to -189 upstream of *GDX1* and *FPH1* ORFs, respectively) and upstream of the *GFA1* ORF (i.e. -174 to -162 and -118 to -106). The motif is also present upstream of *CANPARB_p44920-A* (i.e. -184 to -172), which along with the GP cluster genes is also highly induced in media containing 3-hydroxybenzoate (**Fig 3**).

As our previous studies (7,9,10) indicated that the 3-OAP and GP genes are repressed in media containing glucose, we also searched the promoter sequences for sequence motifs potentially mediating this process. We have found several copies of the SYGGRG motif which is recognized by transcriptional repressors Mig1/Mig2 both in *S. cerevisiae* and *C. albicans* (48-51). Some of these sites (e.g. -139 to -134 and -108 to -103 upstream of *MNX2* and *HBT1* ORFs, respectively) are located near an A/T-box, which is known to be associated with bending of a DNA molecule upon Mig1/Mig2-binding (48) supporting the idea that at least some of the SYGGRG sites are functional in *C. parapsilosis*.

To demonstrate that transcription factors Otf1p and Gtf1p recognize the predicted motifs, we performed EMSA experiments using the protein extracts prepared from the wild type cells (CPL2H1) as well as the mutants lacking a functional copy of the corresponding transcription factor and the labeled ds-oligonucleotide probes OTF1-MNX1 and GTF1-MNX2 derived from the promoters of *MNX1* and *MNX2* genes, respectively. These probes contain a single copy of the predicted binding site. In DNA-binding reactions performed using the extract from the wild type cells we identified one and two bands using the probes OTF1-MNX1 and GTF1-MNX2, respectively (**Fig 9**). As these bands were absent when the extracts were prepared from the mutant cells (i.e. Δ*otf1*/Δ*otf1* for OTF1-MNX1; Δ*gtf1*/Δ*gtf1* for

GTF1-MNX2), we assume that they correspond to the DNA-protein complexes containing the corresponding transcription factor and the probe. To further support this idea, we showed that the 50-fold and higher molar excess of unlabeled oligonucleotide used in the assay as a specific competitor outcompetes the labeled probe from the complex. Importantly, the oligonucleotides OTF1-MNX1_mut and GTF1_MNX2_mut carrying alterations in the conserved positions of predicted binding sites (i.e. $TTTN_{10}TAA$ and $TTTN_7AAA$, respectively), did not interfere with the complex formation.

Taken together, we demonstrate that Otf1p and Gtf1p are Gal4p-like transcription factors present in the extracts from the wild type cells and they specifically bind to DNA fragments carrying the motifs $GGRN_{10}WCC$ and $GGAN_7TCC$, respectively. Gtf1p appears as the main transcriptional activator of the GP gene cluster. On the other hand, although Otf1p contributes to transcriptional activation of the 3-OAP genes, it predominantly controls the expression of *MNX1* encoding decarboxylating mononoxygenase (7,41). This conclusion is supported by differences in the gene expression profiles of the cells grown on 4-hydroxybenzoate compared to those assimilating hydroquinone (**Fig 3**) and the growth phenotypes (**Fig 8**) and underscores the physiological differences in catabolic degradation of hydroxybenzenes and hydroxybenzoates. These results imply that, besides Otf1p, activation of the 3-OAP genes requires additional transcription factor(s). As 4-hydroxybenzoate and hydroquinone differ by the presence of carboxyl group, we speculate that bicarbonate anions generated upon Mnx1p-catalyzed decarboxylation of 4-hydroxybenzoate (**Fig 6B**) and corresponding cellular response may also contribute to identified differences.

Fig 9. Transcription factors Otf1p and Gtf1p bind to predicted sequence motifs.

The EMSA experiments were performed using the protein extracts prepared from CPL2H1 (A),(C), Δ*otf1*/Δ*otf1* (B), and Δ*gtf1*/Δ*gtf1* (D) cells and the 5' end-labeled dsDNA probes containing the predicted Otf1p-binding site from the *MNX1* promoter (OTF1_MNX1; (A),(B)) or the Gtf1p-binding site from the *MNX2* promoter (GTF1_MNX2; (C),(D)). The ds oligonucleotide competitors containing either the wild type (OTF1_MNX1, GTF1_MNX2) or mutated binding motifs (OTF1_MNX1_mut, GTF1_MNX2_mut) were used with increasing amounts of 100, 300, and 500 ng as indicated above lanes.

Phylogenetic analyses. The phylogenetic relationships of the transcription factors Otf1p and Gtf1p, as well as the twelve FAAs in *C. parapsilosis* were first assessed by investigating pre-computed phylogenies and orthology and paralogy relationships in MetaPhORs v2 (52) and PhylomeDB v4 (53) as of October 2020. As Otf1p and Gtf1p display a very sparse distribution among Saccharomycotina, we performed new phylogenetic reconstruction (see Materials and Methods) with the first 250 best Blast hits (e-value < 10^{-20}) in a search against NCBI non-redundant database (as of October 2020). *GTF1* phylogeny (**Fig 10**) closely resembles that previously reported for other genes of the GP cluster such as *GDX1* (9), with a sparse distribution within Saccharomycotina and closely related to Pezizomycotina and Zygomycotina sequences, suggestive of a possible ancient horizontal gene transfer. *OTF1* phylogenetic reconstruction reveals a somewhat broader distribution within Saccharomycotina and a close relationship with Pezizomycotina sequences (**Fig 10**).

Previously we proposed that the 3-OAP variant occurring in *C. parapsilosis* emerged in an ancestral lineage before the divergence of the 'CUG-Ser1' clade from other Saccharomycotina lineages by an upgrade of a shorter version of this pathway (such as seen in *C. albicans*), which allows degradation of only hydroxybenzenes (10). The principal difference between the two variants is the presence of both the Mnx1p-catalyzed decarboxylation step and the functional uptake of hydroxybenzoates provided by Hbt2p and possibly also by its paralogs Hbt3p and Hbt4p, in the longer 3-OAP version. The acquisition of *OTF1* by horizontal gene transfer might have served the need for a specific regulation of this upgraded pathway. Differences in the transcriptional control of *MNX1* and to some extent also *HBT2* and *HBT3* compared to remaining 3-OAP genes (see above) supports the upgrade scenario and provides additional insight into the evolution of this pathway.

Fig 10. Phylogenetic relationships of the transcription factors Gtf1p (left), Otf1p (right), and their closest homologs.

For simplicity, some monophyletic tree partitions including sequences from the same taxonomic classification are collapsed and their number is indicated in brackets. Zygomycotina sequences or partitions are indicated in green, Pezizomycotina sequences and partitions are indicated in red, Saccharomycotina sequences are indicated in black, and the *C. parapsilosis* sequence used as a seed in the blast searches is indicated in blue. Note several *C. albicans* sequences likely correspond to

537 redundant sequences from different strains or sequencing projects. Note as well WP_165932610
538 sequence assigned to a *Bacillus* strain, which could correspond to a taxonomic miss-assignment or
539 contamination. The full phylogenetic trees in newick format, including all sequence names and branch
540 support is provided as supplemental information (**S1 Text**, **S2 Text**).
541
542
543 The evolutionary relationships of the twelve *FAA* genes in *C. parapsilosis* is well represented in
544 PhylomeDB trees (see a simplified example in **S3 Fig**). This reveals an intricate evolution of this family
545 with at least ten nested gene duplications at different ages leading to the twelve paralogs present in *C.*
546 *parapsilosis* and with complex one-to-many orthology and paralogy relationships with the four *FAA*
547 genes present in *S. cerevisiae* and *C. albicans*. This highlights a dynamic gene copy evolution leading
548 to complexification of the FA metabolism in the *C. parapsilosis* clade.
549 Finally, we investigated the possible origin of the putative amidohydrolase gene
550 (*CANPARB_p44920-A* and *CANPARB_p44910-A*) identified in this work. PhylomeDB searches
551 rendered no results, but MetaPhOrs identified an ortholog in *C. metapsilosis* (g2237) sharing 64%
552 protein identity. The *C. metapsilosis* gene has a single reading frame indicating that in *C. parapsilosis*
553 ancestor the gene was split up into two ORFs by an in-frame stop codon UGA. In general, this alteration
554 would inactivate a gene function, although stop codon bypassing or readthrough events (54) could
555 generate a full-length protein corresponding to the polypeptide translated from uninterrupted ORF.
556 Although both *C. parapsilosis* ORFs are transcribed on 3-hydroxybenzoate and the transcript is
557 regulated by transcriptional activator Gtf1p, we did not identify peptides derived neither from individual
558 ORFs nor from a deduced full-length protein by LC-MS/MS analysis. Searches in NCBI non-redundant
559 database identified only bacterial sequences among the top 500 hits, with the best matches belonging
560 to various *Pseudomonas* species with e-values ranging from 10^{-105} to 10^{-102} and sequence identities
561 between 49 and 53% at the protein level. A multiple sequence alignment of the first 100 hits and the
562 two *Candida* sequences revealed conservation of numerous amino acid residues (**S1 Fig**). This result
563 indicates that this gene represents a relatively recent transfer of a gene encoding a putative
564 amidohydrolase to the common ancestor of *C. parapsilosis* and *C. metapsilosis*. Alternatively,
565 considering the relatively low sequence identity between the two transferred genes and their location in
566 different, non-syntenic chromosomal locations in each of the species, two independent origins from a

567 related bacterial donor might be postulated. The low levels of similarity exhibited between the
568 transferred genes and their closest bacterial donors preclude us to pinpoint a specific bacterial species.
569 Interestingly, when limiting the search to Saccharomycotina three significant hits appeared from
570 sequences in the unrelated yeasts *Wickerhamiella sorbophila* (acc.no. XP_024665283.1), *Trichomonascus ciferrii* (KAA8915622.1), and *Naumovozyma castellii* (XP_003673849.1). However,
571
572 their sequence identities with the *C. parapsilosis* protein were lower than that of the bacterial homologs
573 (39%, 35%, and 29%, respectively), suggesting they are more distantly related. Indeed, searches using
574 these other yeast proteins as queries identified other bacteria (for *W. sorbophila*) or non-overlapping
575 species of Pezizomycotina fungi (for *T. ciferrii* and *N. castellii*) among the first 100 significant hits,
576 suggesting each of these yeasts acquired a different amidohydrolase gene in independent horizontal
577 gene transfers. Such recurrent horizontal gene transfer scenario is reminiscent of other metabolic genes
578 including amino acid racemases, which are also present in *C. parapsilosis* and other yeast species (55).

Materials and Methods

Yeast strains. *C. parapsilosis* strains CLIB214 (identical to the type strain CBS604), CPL2H1 (CLIB214 Δ*leu2*/Δ*leu2,* Δ*his1*/Δ*his1*; (56)), its mutant derivatives (Δ*gtf1*/Δ*gtf1* and Δ*otf1*/Δ*otf1*; this study), CDU1 (CLIB214 Δ*ura3*/Δ*ura3*; (57)), and SR23 met1$^-$ (*ade$^-$, lys4$^-$, met1$^-$*; (58)) were used in this study.

DNA isolation and sequencing. Genomic DNA was isolated from the strain CLIB214. Briefly, a yeast culture grown overnight at 28 °C in 100 ml of YPD medium (1% [wt/vol] yeast extract, 2% [wt/vol] peptone, 2% [wt/vol] glucose) at 28 °C was harvested by centrifugation (5 min, 2,100 *g* at 4 °C), the cells were resuspended in 20 ml of 2% [vol/vol] 2-mercaptoethanol and incubated for 30 min at room temperature. The spheroplasts were prepared in 6 ml of 1 M sorbitol, 10 mM EDTA (pH 8.0) containing 0.125 mg of Zymolyase 20T (Seikagaku) at 37 °C, pelleted by centrifugation (5 min, 2,100 *g* at 4 °C) and lysed in 3 ml of 0.15 M NaCl, 0.1 M EDTA (pH 8.0), 0.1% [wt/vol] SDS. Proteins were removed by three extractions with equal volume of phenol buffered with 10 mM Tris-HCl, 1 mM EDTA (pH 8.0) and by one extraction with equal volume of chloroform : isoamyl alcohol (24 : 1). Nucleic acids were precipitated using 0.1 M NaCl and 1 volume of 96% [vol/vol] ethanol, pelleted by centrifugation (10 min, 16,100 *g* at 4 °C), washed with 70% [vol/vol] ethanol and air dried. The precipitate was dissolved in 1 ml of 10 mM Tris-HCl, 1 mM EDTA (pH 7.5), 0.1 mg/ml RNase A and incubated for 45 min at 37 °C. DNA was extracted by phenol and chloroform : isoamyl alcohol, precipitated using 0.1 M NaCl and 2 volumes of 96% [vol/vol] ethanol, washed with 70% [vol/vol] ethanol, air dried, dissolved in 150 µl 10 mM Tris-HCl, 1 mM EDTA (pH 7.5) and purified on a Genomic-tip 100/G (Qiagen) according to the manufacturer's instructions. A paired-end (2×151-nt) TruSeq PCR-free DNA library was sequenced on a NovaSeq6000 platform at Macrogen Korea, yielding 81,578,508 reads (12.32 Gbp; 944x coverage). Nanopore sequencing was performed on a MinION Mk-1B device with an R9.4.1 flow cell using a Rapid barcoding kit (SQK-RBK004; Oxford Nanopore Technologies). 119,788 reads were obtained (mean and median lengths are 9,200.2 and 5,938 nucleotides, respectively) totaling 1.1 GBp (84x coverage). Nanopore reads were assembled by Canu version 1.9 (59), resulting in 20 contigs, which were manually examined. Chromosomes 1, 2, 3, 4 and 7 were used as assembled by Canu. Chromosome 8 was created by connecting two Canu contigs. In the contig corresponding to chromosome 5, a 8 kbp region was replaced by a longer 14.5 kb version from one of the excluded shorter contigs. This region

609 contains two copies of the *PDR5* gene, possibly with a copy number variation. Finally, regions directly
610 upstream and downstream of ribosomal DNA (rDNA) arrays on chromosome 6 were misassembled in
611 the Canu assembly. These regions were replaced by sequences assembled from Illumina reads by
612 SPAdes version 3.12 (60). After these manual modifications, the entire assembly was polished first by
613 Medaka version 0.11.5 (61) using nanopore reads, and then by three iterations of Pilon version 1.12
614 (62). The rDNA repeat poses problems for polishing due to its repetitive nature, and thus a single copy
615 of the repeat was polished separately by Pilon and then used in the final assembly. Mitochondrial DNA
616 was taken from the GenBank acc. no. DQ376035.2. A whole genome alignment to the reference
617 genome sequence from the strain CDC317 (GCA_000182765.2; (21,63)) was computed by Last
618 version 830 (64) followed by last-split to assign to each portion of CDC317 sequence a unique position
619 in our assembly. To annotate protein coding genes, the genes from the strain CDC317 were aligned to
620 our assembly by Blat version v. 36x2 (65) and supplied as hints to Augustus version 3.2.3 (66).
621 Augustus was run originally with parameters for *Candida albicans*, then retrained on the predictions
622 matching CDC317 genes. Disagreements with CDC317 annotation were manually inspected, and as
623 a result, 61 genes were modified, 12 genes removed and 72 genes added.
624
625 **Electrophoretic karyotyping.** About $1x10^9$ cells of the strain CLIB214 grown overnight in a YPD
626 medium were resuspended in 0.5 ml of 1.2 M sorbitol, 40 mM citric acid, 120 mM disodium phosphate,
627 20 mM EDTA (pH 8.0), 5 mM DTT, 0.2 mg/ml zymolyase 20T (Seikagaku) and incubated for 90 min at
628 37 °C. Protoplasts were then harvested by centrifugation (1 min, 2,100 *g*), resuspended in 1 ml of molten
629 1% [wt/vol] low melting point agarose in 50 mM EDTA (pH 8.5) cooled to 45 °C and poured into the
630 sample forms. The agarose embedded samples were incubated for 30 min at 37 °C in 10 mM Tris.Cl,
631 0.5 M EDTA (pH 8.5) and then overnight at 50 °C in 1% [wt/vol] N-lauroylsarcosine, 0.5 M EDTA (pH
632 8.5), 0.5 mg/ml proteinase K. Pulsed-field gel electrophoresis (PFGE) was performed in a CHEF
633 Mapper XA Chiller System (Bio-Rad) with 120° angle between the electric fields at the following settings:
634 (I) 120 s pulses for 24 h followed by 240 s pulses for 36 h at 4.5 V/cm; (II) 120 s pulses for 20 h followed
635 by 240 s pulses for 28 h at 4 V/cm; (III): 60 s pulses for 15 hours followed by 90 s pulses for 9 hours at
636 6 V/cm. The samples were separated in 0.8% (settings I and II) or 1% [wt/vol] agarose gels (settings
637 III) in 0.5x TBE buffer (45 mM Tris-borate, 1 mM EDTA, pH 8.0) at 14 °C, throughout. After PFGE, the

638 gels were stained with ethidium bromide (0.5 µg/ml) for 45 min and washed in water for additional 45
639 min.
640
641 **RNA-Seq analysis.** *C. parapsilosis* CLIB214 was pre-cultivated in an SD medium (0.67% [wt/vol] yeast
642 nitrogen base w/o amino acids (Difco), 2% [wt/vol] glucose) for 24 h at 28 °C, then washed in water
643 and re-grown in SMix10 medium (0.67% [wt/vol] yeast nitrogen base w/o amino acids (Difco), 3.3 mM
644 3-hydroxybenzoate, 3.3 mM 4-hydroxybenzoate, and 3.3 mM hydroquinone) for additional 24 h at 28
645 °C. The pre-culture was inoculated (OD_{600} ~ 0.3) in triplicates into synthetic media (0.67% [wt/vol] yeast
646 nitrogen base w/o amino acids (Difco)) containing 2% [wt/vol] galactose (SGal) or 10 mM
647 hydroxyaromatic compound (i.e. 3-hydroxybenzoate (S3OH), 4-hydroxybenzoate (S4OH) or
648 hydroquinone (SHyd)) as a sole carbon source and cultivated at 28 °C till OD_{600} ~ 1. The consumption
649 of hydroxyaromatic compounds in the cultivation media was analyzed spectrophotometrically (**S9 Fig**).
650 The cultures of CPL2H1, Δ*gtf1*/Δ*gtf1,* and Δ*otf1*/Δ*otf1* were prepared similarly, except that the
651 cultivation media were supplemented with leucine (20 µg/ml) and histidine (20 µg/ml) and the cells were
652 grown in SMix15 medium (0.67% [wt/vol] yeast nitrogen base w/o amino acids (Difco), 5 mM 3-
653 hydroxybenzoate, 5 mM 4-hydroxybenzoate, and 5 mM hydroquinone). Total RNA was isolated by
654 extraction with hot acid phenol essentially as described in (67) and purified using an RNeasy mini kit
655 (Qiagen) according to the manufacturer's instructions. Transcriptome sequencing reads were
656 generated from TruSeq stranded mRNA LT paired-end (2×151-nt) libraries on a NovaSeq6000 platform
657 at Macrogen Korea. Reads were processed with Trimmomatic 0.39 (68) and mapped to the CLIB214
658 genome sequence using HiSat2 2.1.0 (69). Duplicated reads were removed using samtools rmdup and
659 the coverage was calculated using samtools depth (samtools version 1.9; (70)). Differential gene
660 expression analysis was performed using the Geneious 11.1.5 package (Biomatters); the DESeq2
661 method (71) was used for samples in biological triplicates (*i.e.* CLIB214 grown in SGal, S3OH, S4OH,
662 and SHyd media), the Geneious method was used for comparisons of CPL2H1 vs. Δ*gtf1*/Δ*gtf1* and
663 CPL2H1 vs. Δ*otf1*/Δ*otf1* grown in SMix15 medium. Heatmaps were generated using the pheatmap
664 package 1.0.12 (https://CRAN.R-project.org/package=pheatmap; (72)). Gene ontology and KEGG
665 database searches were performed using the Candida Genome Database GO Slim Mapper and Term
666 Finder (http://www.candidagenome.org) and the KEGG mapper
667 (https://www.genome.jp/kegg/tool/map_pathway.html), respectively.

668

669 **Analyses of cultivation media.** The consumption of hydroxyaromatic compounds and pH in cultivation
670 media were analyzed before and at the end of cultivation using a Multiskan GO spectrophotometer
671 (Thermo Scientific) and PH CHECK pH meter (Dostmann Electronic), respectively. The measurements
672 were performed at room temperature. Following absorption maxima and media dilutions were used in
673 the substrate consumption analyses; A_{max}=297 nm, 2-fold dilution (3-hydroxybenzoate), A_{max}=255 nm,
674 20-fold dilution (4-hydroxybenzoate), and A_{max}=290 nm, 5-fold dilution (hydroquinone). To monitor pH
675 changes during cultivations, synthetic media (see above) varying by the carbon source were
676 supplemented with 0.01% [wt/vol] bromothymol blue and adjusted to pH 6.1-6.4 with NaOH. The
677 cultures were inoculated to 6×10^6 cells/ml and grown at 28 °C to mid exponential phase. Cell-free media
678 were used as a control. To document color, the cultures were centrifuged (1 min, 2,100 *g*) to remove
679 the cells and 100 µl of cultivation media were transferred into wells of a 96-well plate and photographed
680 using a Nikon D7000 camera.

681

682 **Proteomic analysis.** Protein extracts were prepared in triplicates from *C. parapsilosis* CLIB214 cells
683 pre-cultivated overnight at 28 °C in an S3OH medium, inoculated (5×10^6 cells/ml) to SGal, S3OH,
684 S4OH, and SHyd media and grown at 28 °C till ~ 10^7 cells/ml. The cells were harvested by centrifugation
685 (5 min, 2,100 *g* at 4 °C), resuspended in 50 mM Tris-HCl (pH 8.8), 1 mM EDTA (pH 8.0) and
686 homogenised using FastPrep-24 (MP Biomedicals). Cell debris was removed by centrifugation (15 min,
687 16,000 *g* at 4 °C) and protein concentration was determined using Bradford`s method (73). For LC-
688 MS/MS analysis, protein aliquots (50 µg) were diluted in 100 µl of 25 mM Tris-HCl (pH 7.8), 0.1 mM
689 $CaCl_2$, treated using 5 mM dithiothreitol for 30 min at 60 °C and alkylated in 40 mM chloroacetamide for
690 1 hour at 37 °C. The proteins were digested overnight by trypsin (1:30 [wt/wt]) at 37 °C. Acidified (0.5%
691 [vol/vol] trifluoroacetic acid (TFA)) peptide solution was clarified by centrifugation and purified on a
692 microtip C18 SPE. The concentration of eluted peptides was determined by Pierce™ Quantitative
693 Fluorometric Peptide Assay (Thermo Scientific). The peptides were dissolved in 0.1% [vol/vol] TFA and
694 2% [vol/vol] acetonitrile (ACN), loaded (500 ng per run) onto a trap column (PepMap100 C18, 300 µm
695 x 5 mm, Dionex, CA, USA) and separated with an EASY-Spray C18 column (75 µm x 500 mm, Thermo
696 Scientific) on Ultimate 3000 RSLCnano system (Dionex) in a 120-minute gradient (3-43% B), curve 7,
697 and flow-rate 250 nl/min. The two mobile phases were used: 0.1% [vol/vol] formic acid (A) and 80%

[vol/vol] ACN with 0.1% [vol/vol] formic acid (B). Eluted peptides were sprayed directly into Orbitrap Elite mass spectrometer (Thermo Scientific, MA, USA) and spectral datasets were collected in the data dependent mode using Top15 strategy for the selection of precursor ions for the HCD fragmentation (74). Each of the three experimental replicates was analysed in technical triplicates. Protein spectra were analyzed by MaxQuant software (version 1.6.17.0) using carbamidomethylation (C) as permanent and oxidation (M) and N-terminal acetylation as variable modifications, with engaged 'match between the runs' feature and label-free quantification (LFQ) and further examined in Perseus version 1.6.15.0 (75,76). The search was performed against the *C. parapsilosis* CLIB214 protein database containing 5856 entries. Proteins were evaluated and annotated based on information from CDC317 strain orthologs. Contaminating peptides, reverse peptides and peptides only identified by site were removed, then the protein entries were further filtered to have at least two LFQ values in at least one of the biological conditions (different carbon sources). Following an imputation, differentially expressed proteins were identified by ANOVA test (permutation-based FDR 0.01).

Preparation of knockout strains. The mutants lacking either *GTF1* or *OTF1* gene were generated in the strain CPL2H1 essentially as described in (56,77). Deletion constructions contained the upstream (UpFw primer and UpRev primer; **S4 Table**) and downstream (DownFw primer and DownRev primer) homologous regions of the target ORF and either *Candida dubliniensis HIS1* or *Candida maltosa LEU2* sequences as selection markers. For selection marker amplification the primers 'pSN52/pSN40 Fw' and 'pSN52/pSN40 Rev' were used. DownFw, UpRev, and the primers used for marker amplification also harbored fusion sequences for later fragment joining. The reverse primer ('pSN52/pSN40 Rev') used for marker amplification also carried a TAG sequence between the mentioned fusion sequences. Deletion cassettes were transformed into CPL2H1 strain and the transformants were plated onto selective media. Heterozygous mutants were obtained and used to prepare homozygous mutants. Mutant strains were verified by colony polymerase chain reaction (PCR) using the primers specific for both the marker sequences and the outside of the integration sites at both the upstream and downstream homologous regions. The ORF specific primer '5'- check primer' was used as forward primer together with '*LEU1/HIS1 primer*' as reverse primer, while the ORF specific primer '3'- check primer' was applied as reverse primer together with the '*LEU2/HIS2* primer' as forward primer.

Assimilation tests of the wild type and mutant strains were performed on solid synthetic media (0.67% [wt/vol] yeast nitrogen base w/o amino acids (Difco), 2% [wt/vol] agar, 30 µg/ml leucine, 20 µg/ml histidine) differing by the carbon source (i.e. 2% [wt/vol] glucose (SD), 10 mM 3-hydroxybenzoate (S3OH), 10 mM 4-hydroxybenzoate (S4OH), 10 mM 2,4-dihydroxybenzoate (S24diOH), 10 mM 2,5-dihydroxybenzoate (S25diOH), 10 mM 3,4-dihydroxybenzoate (S34diOH), 10 mM hydroquinone (SHyd) or 10 mM resorcinol (SRes)). Prior to the addition to the media, hydroxyaromatic compounds were dissolved in dimethyl sulfoxide (DMSO) as 0.5 M stocks.

Fluorescence microscopy. The cells were observed using a BX50 microscope with the appropriate filter set and a digital camera DP70 (Olympus Optical). To visualize peroxisomes in *C. parapsilosis* cells, we constructed a plasmid pBP7-mCherry-SKL expressing the mCherry protein tagged with peroxisomal targeting signal 'SKL' at its C-terminus and a control plasmid pBP7-mCherry expressing the unmodified protein. The mCherry coding sequence was amplified by PCR using the primers shown in **S4 Table** and the plasmid pMG2254 (39) as a template. The PCR products were inserted into the *Xba*I site of the pBP7 vector (78) using a Gibson assembly cloning kit (New England Biolabs). The cloned genes are placed downstream of the *GAL1* promoter in the resulting plasmid constructs. The constructs were transformed into *C. parapsilosis* cells CDU1 by the standard protocol (79). The transformants were cultivated overnight in liquid synthetic medium (0.67% [wt/vol] yeast nitrogen base w/o amino acids (Difco)) containing 2% [wt/vol] glucose (SD) at 28 °C. The cells were then inoculated to synthetic media differing by the carbon source (i.e. 2% [wt/vol] galactose (SGal), 10 mM 3-hydroxybenzoate (S3OH), 10 mM 4-hydroxybenzoate (S4OH)), cultivated for 24 hour (SGal), 48 hours (S3OH) or 72 hours (S4OH) at 28 °C and examined by fluorescence microscopy. To investigate the intracellular localization of Gtf1p and Otf1p, we constructed yEGFP3-tagged versions of both proteins as follows. The coding sequences of *GTF1* and *OTF1* were PCR-amplified from the CLIB214 genomic DNA using gene specific primers (**S4 Table**) and the PCR products were inserted into the *Sma*I site of the pPK6 vector (78) using a Gibson assembly cloning kit (New England Biolabs). This allows the expression of cloned genes under the control of the *GAL1* promoter. The plasmid constructs were transformed into *C. parapsilosis* cells SR23 met1$^-$ as described in (79). The transformants were grown overnight in SGal medium (0.67% [wt/vol] yeast nitrogen base w/o amino acids (Difco), 1% [wt/vol]

galactose) at 28 °C. Prior to fluorescent microscopy, the cellular DNA was stained with 4′,6-diamidino-2-phenylindole (DAPI, 1 µg/ml) for 20 min.

Electrophoretic Mobility Shift Assay (EMSA). The wild type (CPL2H1) and mutant (Δ*gtf1*/Δ*gtf1*, Δ*otf1*/Δ*otf1*) cells were grown in synthetic media containing combinations of hydroxyaromatic substrates (i.e. 7.5 mM 3-hydroxybenzoate and 7.5 mM 4-hydroxybenzoate (wild type); 2.5 mM 3-hydroxybenzoate, 2.5 mM 4-hydroxybenzoate, and 10 mM hydroquinone (Δ*gtf1*/Δ*gtf1*); 10 mM 3-hydroxybenzoate and 5 mM 4-hydroxybenzoate (Δ*otf1*/Δ*otf1*)) supplemented with leucine (40 µg/ml) and histidine (40 µg/ml). Protein extracts were prepared according to Winkler *et al.* (80) with some modifications. Ice-cold solutions were used throughout the experiment and all incubations were performed on ice. Cells were harvested at exponential growth phase by centrifugation (10 min, 3,600 *g* at 4 °C), washed with water, resuspended in 5 volumes of 200 mM Tris-HCl (pH 8.0), 400 mM $(NH_4)_2SO_4$, 10 mM $MgCl_2$, 1 mM EDTA, 7 mM 2-mercaptoethanol, 10% [vol/vol] glycerol, 1 mM phenylmethylsulfonyl fluoride (PMSF), 1 × cOmplete™ protease inhibitor cocktail tablet (Roche Applied Science). The cells were disrupted by vortexing with glass-beads (0.45-0.5 mm in diameter, 0.8 g/ml) 7 times for 1 min with intermittent cooling on ice for 1 min. Lysates were incubated for 30 min, centrifuged at 9,000 *g* for 60 min and proteins in supernatant were precipitated by addition of $(NH_4)_2SO_4$ in 10 mM HEPES (pH 8.0), 5 mM EDTA, 1 mM PMSF for 30 min (the final concentration of $(NH_4)_2SO_4$ was 40% [wt/vol] in total volume of 1.5 ml). The sample was centrifuged at 9,000 *g* for 15 min and the pellet was resuspended in 100 – 150 µl of 10 mM HEPES (pH 8.0), 5 mM EDTA, 7 mM 2-mercaptoethanol, 20% [vol/vol] glycerol, 1 mM PMSF, 1× cOmplete™ protease inhibitor cocktail tablet (Roche Applied Science). The protein extracts were stored at -80 °C prior to the use in DNA-binding assays. Oligonucleotide probes were prepared as follows. Direct strand oligonucleotides (**S4 Table**) were labeled at 5′ end by T4 polynucleotide kinase (Thermo Scientific) and [γ-^{32}P]ATP (Hartmann Analytic), mixed with 3-fold molar excess of the unlabeled complementary oligonucleotide, heated at 100 °C for 10 min and slowly cooled down to room temperature to allow efficient formation of the double-stranded probes. The probes were purified using Illustra™ MicroSpin™ G-25 Columns (GE Healthcare). The DNA binding assays were carried out in 10 µl of 10 mM Tris-HCl (pH 7.5), 50 mM NaCl, 0.1 mM EDTA containing 15 µg of proteins, 2 ng of the ^{32}P-labeled probe, 2 µg of poly(dA-dC) • poly(dG-dT). Unlabeled double-stranded oligonucleotides were used as specific competitors. The reaction mixtures were

786 incubated for 15 min at room temperature and immediately loaded on 5% polyacrylamide gels in TG
787 buffer (25 mM Tris-HCl (pH 8.3), 192 mM glycine). The electrophoresis was performed at 4 °C in the
788 TG buffer at 10 V/cm for 90 min. Gels were fixed with 10 ml of 10% [vol/vol] methanol, 10% [vol/vol]
789 acetic acid for 10 min, dried and exposed to the storage phosphor screen. Signal was detected using a
790 Personal Molecular Imager FX (Bio-Rad).
791
792 **Phylogenetic analysis.** Sequences were aligned with Muscle v3.8 (81) with default parameters and
793 maximum likelihood phylogenetic trees were built using Iqtree v2.0 (82) allowing full exploration of
794 model parameters and estimating the support of tree partitions using ultrafast bootstrap support with
795 1000 iterations (83). Orthology and paralogy relationships, as well as duplication nodes were inferred
796 with the species overlap algorithm (84), with the relative age inferred from topological analysis (85).
797 Blast searches were performed at NCBI website (https://blast.ncbi.nlm.nih.gov/) using default
798 parameters unless indicated otherwise.
799
800 **Data availability.** The CLIB214 genome assembly, nanopore and Illumina reads were deposited in the
801 European Nucleotide Archive (ENA) under the project PRJEB37287. RNA-Seq data were submitted to
802 ArrayExpress under the accessions E-MTAB-9442 and E-MTAB-9443. The mass spectrometry
803 proteomics data have been deposited to the ProteomeXchange Consortium via the PRIDE (86) partner
804 repository with the dataset identifier PXD024608 and 10.6019/PXD024608.

References

1. Slot JC. Fungal gene cluster diversity and evolution. Adv Genet. 2017;100:141–78.
2. Nützmann HW, Scazzocchio C, Osbourn A. Metabolic Gene Clusters in Eukaryotes. Annu Rev Genet. 2018;52:159–83.
3. Vesth TC, Brandl J, Andersen MR. FunGeneClusterS: Predicting fungal gene clusters from genome and transcriptome data. Synth Syst Biotechnol. 2016;1:122–9.
4. Töpfer N, Fuchs LM, Aharon A. The PhytoClust tool for metabolic gene clusters discovery in plant genomes. Nucleic Acids Res. 2017;45:7049–63.
5. Marcet-Houben M, Gabaldón T. Evolutionary and functional patterns of shared gene neighbourhood in fungi. Nat Microbiol. 2019;4:2383–92.
6. Wisecaver JH, Rokas A. Fungal metabolic gene clusters-caravans traveling across genomes and environments. Front Microbiol. 2015;6:161.
7. Holesova Z, Jakubkova M, Zavadiakova I, Zeman I, Tomaska L, Nosek J. Gentisate and 3-oxoadipate pathways in the yeast *Candida parapsilosis*: identification and functional analysis of the genes coding for 3-hydroxybenzoate 6-hydroxylase and 4-hydroxybenzoate 1-hydroxylase. Microbiology (Reading). 2011;157:2152–63.
8. Gerecova G, Nebohacova M, Zeman I, Pryszcz LP, Tomaska L, Gabaldón T, et al. Metabolic gene clusters encoding the enzymes of two branches of the 3-oxoadipate pathway in the pathogenic yeast *Candida albicans*. FEMS Yeast Res. 2015;15:fov006.
9. Zeman I, Neboháčová M, Gérecová G, Katonová K, Jánošíková E, Jakúbková M, Centárová I, Dunčková I, Tomáška L, Pryszcz LP, Gabaldón T, Nosek J. Mitochondrial carriers link the catabolism of hydroxyaromatic compounds to the central metabolism in *Candida parapsilosis*. G3 (Bethesda). 2016;6:4047–58.
10. Cillingová A, Zeman I, Tóth R, Neboháčová M, Dunčková I, Hölcová M, Jakúbková M, Gérecová G, Pryszcz LP, Tomáška Ľ, Gabaldón T, Gácser A, Nosek J. Eukaryotic transporters for hydroxyderivatives of benzoic acid. Sci Rep. 2017;7:8998.
11. Vrzoňová R, Tóth R, Siváková B, Moťovská A, Gaplovská K, Baráth P, et al. OCT1 - a yeast mitochondrial thiolase involved in the 3-oxoadipate pathway. FEMS Yeast Res. 2021;21: foab034.

12. Mixão V, Hegedűsová E, Saus E, Pryszcz LP, Cillingová A, Nosek J, et al. Genome assembly of *Candida subhashii* reveals its hybrid nature and dual mitochondrial genome conformation. DNA Res. 2021;28:dsab006.
13. Middelhoven WJ, Coenen A, Kraakman B, Sollewijn Gelpke MD. Degradation of some phenols and hydroxybenzoates by the imperfect ascomycetous yeasts *Candida parapsilosis* and *Arxula adeninivorans*: evidence for an operative gentisate pathway. Antonie van Leeuwenhoek 1992;62:181–7.
14. Eppink MH, Cammaart E, Van Wassenaar D, Middelhoven WJ, van Berkel WJ. Purification and properties of hydroquinone hydroxylase, a FAD-dependent monooxygenase involved in the catabolism of 4-hydroxybenzoate in *Candida parapsilosis* CBS604. Eur J Biochem. 2000;267:6832–40.
15. Csonka K, Vadovics M, Marton A, Vágvölgyi C, Zajta E, Tóth A, et al. Investigation of OCH1 in the virulence of *Candida parapsilosis* using a new neonatal mouse model. Front Microbiol. 2017;8:1197.
16. Turner SA, Ma Q, Ola M, Martinez de San Vicente K, Butler G. Dal81 regulates expression of arginine metabolism genes in *Candida parapsilosis.* mSphere 2018;3:e00028-18.
17. Nguyen TN, Dubreucq E, Perrier V, Tran QH, Charpentier C, Charnay C, Terki F, et al. Interactions between *trans*-resveratrol and *Cp*LIP2 lipase/acyltransferase: Evidenced by fluorescence and *in silico.* Food Chem. 2020;318:126482.
18. Pál SE, Tóth R, Nosanchuk JD, Vágvölgyi C, Németh T, Gácser A. A *Candida parapsilosis* overexpression collection reveals genes required for pathogenesis. J Fungi (Basel) 2021;7:97.
19. Ashford B. Certain conditions of the gastrointestinal tract in Puerto Rico and their relation to tropical sprue. Am J Trop Med Hyg. 1928;8**:**507–38.
20. Logue ME, Wong S, Wolfe KH, Butler G. A genome sequence survey shows that the pathogenic yeast *Candida parapsilosis* has a defective MTLa1 allele at its mating type locus. Eukaryot Cell 2005;4**:**1009–17.
21. Butler G, Rasmussen MD, Lin MF, Santos MAS, Sakthikumar S, Munro CA, et al. Evolution of pathogenicity and sexual reproduction in eight *Candida* genomes. Nature 2009;459:657–62.
22. Van Roermund CWT, Waterham HR, Ijlst L, Wanders RJA. Fatty acid metabolism in *Saccharomyces cerevisiae*. Cell Mol Life Sci. 2003;60:1838–51.

23. Hashimoto F, Hayashi H. Significance of catalase in peroxisomal fatty acyl-CoA beta-oxidation: NADH oxidation by acetoacetyl-CoA and H_2O_2. J Biochem. 1990;108:426–31.
24. Black PN, DiRusso CC. Yeast acyl-CoA synthetases at the crossroads of fatty acid metabolism and regulation. Biochim Biophys Acta - Mol Cell Biol Lipids 2007;1771:286–98.
25. Kunze M, Pracharoenwattana I, Smith SM, Hartig A. A central role for the peroxisomal membrane in glyoxylate cycle function. Biochim Biophys Acta - Mol Cell Res. 2006;1763:1441–52.
26. Cartwright JL, Gasmi L, Spiller DG, McLennan AG. The *Saccharomyces cerevisiae PCD1* gene encodes a peroxisomal nudix hydrolase active toward coenzyme A and its derivatives. J Biol Chem. 2000;275:32925–30.
27. Strijbis K, Distel B. Intracellular acetyl unit transport in fungal carbon metabolism. Eukaryot Cell. 2010;9:1809–15.
28. Beyer A, Hollunder J, Nasheuer HP, Wilhelm T. Post-transcriptional expression regulation in the yeast *Saccharomyces cerevisiae* on a genomic scale. Mol Cell Proteomics. 2004;3:1083–92.
29. Wu G, Nie L, Zhang W. Integrative analyses of posttranscriptional regulation in the yeast *Saccharomyces cerevisiae* using transcriptomic and proteomic data. Curr Microbiol. 2008;57:18–22.
30. Pronk JT, Yde Steensma H, Van Dijken JP. Pyruvate metabolism in *Saccharomyces cerevisiae*. Yeast 1996;12:1607–33.
31. Carman AJ, Vylkova S, Lorenz MC. Role of acetyl coenzyme A synthesis and breakdown in alternative carbon source utilization in *Candida albicans*. Eukaryot Cell 2008;7:1733–41.
32. Otzen C, Bardl B, Jacobsen ID, Nett M, Brock M. *Candida albicans* utilizes a modified β-oxidation pathway for the degradation of toxic propionyl-CoA. J Biol Chem. 2014;289:8151–69.
33. Evers ME, Höhfeld J, Kunau WH, Harder W, Veenhuis M. Physiological studies on the utilization of oleic acid by *Saccharomyces cerevisiae* in relation to microbody development. FEMS Microbiol Lett. 1991;69:73-8.
34. Thoms S, Erdmann R. Dynamin-related proteins and Pex11 proteins in peroxisome division and proliferation. FEBS J. 2005;272:5169–81.
35. Koch J, Brocard C. Membrane elongation factors in organelle maintenance: the case of peroxisome proliferation. Biomol Concepts 2011;2:353–364.

892 36. Jansen RLM, van der Klei IJ. The peroxisome biogenesis factors Pex3 and Pex19: multitasking
893 proteins with disputed functions. FEBS Lett. 2019;593:457–474.
894 37. Walter T, Erdmann R. Current Advances in Protein Import into Peroxisomes. Protein J. 2019;
895 38:351–362.
896 38. Knoblach B, Rachubinski RA. How peroxisomes partition between cells. A story of yeast,
897 mammals and filamentous fungi. Curr Opin Cell Biol. 2016;41:73–80.
898 39. Gerami-Nejad M, Dulmage K, Berman J. Additional cassettes for epitope and fluorescent fusion
899 proteins in *Candida albicans.* Yeast 2009;26:399–406.
900 40. van Berkel WJ, Eppink MH, Middelhoven WJ, Vervoort J, Rietjens IM. Catabolism of 4-
901 hydroxybenzoate in *Candida parapsilosis* proceeds through initial oxidative decarboxylation by a
902 FAD-dependent 4-hydroxybenzoate 1-hydroxylase. FEMS Microbiol Lett. 1994;121:207–15.
903 41. Eppink MH, Boeren SA, Vervoort J, van Berkel WJ. Purification and properties of 4-
904 hydroxybenzoate 1-hydroxylase (decarboxylating), a novel flavin adenine dinucleotide-dependent
905 monooxygenase from *Candida parapsilosis* CBS604. J Bacteriol. 1997;179:6680–7.
906 42. Kotyk A, Lapathitis G, Křenková Š. Glucose- and K(+)-induced acidification in different yeast
907 species. Folia Microbiol. 1999;44:295–8.
908 43. Martin R, Pohlers S, Mühlschlegel FA, Kurzai O. CO_2 sensing in fungi: at the heart of metabolic
909 signaling. Curr Genet. 2017;63:965–72.
910 44. MacPherson S, Larochelle M, Turcotte B. A fungal family of transcriptional regulators: the zinc
911 cluster proteins. Microbiol Mol Biol Rev. 2006;70:583–604.
912 45. Todd RB, Andrianopoulos A. Evolution of a fungal regulatory gene family: the Zn(II)2Cys6
913 binuclear cluster DNA binding motif. Fungal Genet Biol. 1997;21:388–405.
914 46. Baum JA, Geever R, Giles NH. Expression of *qa-1F* activator protein: identification of upstream
915 binding sites in the *qa* gene cluster and localization of the DNA-binding domain. Mol Cell Biol.
916 1987;7:1256–66.
917 47. Bailey TL, Boden M, Buske FA, Frith M, Grant CE, Clementi L, et al. MEME SUITE: tools for motif
918 discovery and searching. Nucleic Acids Res. 2009;37:W202–8.
919 48. Lundin M, Nehlin JO, Ronne H. Importance of a flanking AT-rich region in target site recognition
920 by the GC box-binding zinc finger protein MIG1. Mol Cell Biol. 1994;14:1979–85.

49. Zaragoza O, Rodríguez C, Gancedo C. Isolation of the *MIG1* gene from *Candida albicans* and effects of its disruption on catabolite repression. J Bacteriol. 2000;182:320–6.
50. Murad AM, d'Enfert C, Gaillardin C, Tournu H, Tekaia F, Talibi D, et al. Transcript profiling in *Candida albicans* reveals new cellular functions for the transcriptional repressors *Ca*Tup1, *Ca*Mig1 and *Ca*Nrg1. Mol Microbiol. 2001;42:981–93.
51. Lagree K, Woolford CA, Huang MY, May G, McManus CJ, Solis NV, et al. Roles of *Candida albicans* Mig1 and Mig2 in glucose repression, pathogenicity traits, and *SNF1* essentiality. PLoS Genet. 2020;16:e1008582.
52. Chorostecki U, Molina M, Pryszcz LP, Gabaldón T. MetaPhOrs 2.0: integrative, phylogeny-based inference of orthology and paralogy across the tree of life. Nucleic Acids Res. 2020;48:W553–7.
53. Huerta-Cepas J, Capella-Gutiérrez S, Pryszcz LP, Marcet-Houben M, Gabaldón T. PhylomeDB v4: zooming into the plurality of evolutionary histories of a genome. Nucleic Acids Res. 2014;42:D897–902.
54. von der Haar T, Tuite MF. Regulated translational bypass of stop codons in yeast. Trends Microbiol. 2007;15:78–86.
55. Naranjo-Ortíz MA, Brock M, Brunke S, Hube B, Marcet-Houben M, Gabaldón T. Widespread inter- and intra-domain horizontal gene transfer of d-amino acid metabolism enzymes in eukaryotes. Front Microbiol. 2016;7:2001.
56. Holland LM, Schröder MS, Turner SA, Taff H, Andes D, Grózer Z, et al. Comparative phenotypic analysis of the major fungal pathogens *Candida parapsilosis* and *Candida albicans*. PLoS Pathog. 2014;10:e1004365.
57. Ding C, Butler G. Development of a gene knockout system in *Candida parapsilosis* reveals a conserved role for BCR1 in biofilm formation. Eukaryot Cell. 2007;6:1310–19.
58. Nosek J, Adamikova L, Zemanova J, Tomaska L, Zufferey R, Mamoun CB. Genetic manipulation of the pathogenic yeast *Candida parapsilosis*. Curr Genet. 2002;42:27–35.
59. Koren S, Walenz BP, Berlin K, Miller JR, Bergman NH, Phillippy AM. Canu: scalable and accurate long-read assembly via adaptive k-mer weighting and repeat separation. Genome Res. 2017;27:722–36.

60. Bankevich A, Nurk S, Antipov D, Gurevich AA, Dvorkin M, Kulikov AS, et al. SPAdes: a new genome assembly algorithm and its applications to single-cell sequencing. J Comput Biol. 2012;19:455–77.
61. Oxford Nanopore Technologies. Medaka. 2020. Available from: https://github.com/nanoporetech/medaka
62. Walker BJ, Abeel T, Shea T, Priest M, Abouelliel A, Sakthikumar S, et al. Pilon: an integrated tool for comprehensive microbial variant detection and genome assembly improvement. PLoS ONE 2014;9:e112963.
63. Guida A, Lindstädt C, Maguire SL, Ding C, Higgins DG, Corton NJ, et al. Using RNA-seq to determine the transcriptional landscape and the hypoxic response of the pathogenic yeast *Candida parapsilosis*. BMC Genomics 2011;12:628.
64. Frith MC, Kawaguchi R. Split-alignment of genomes finds orthologies more accurately. Genome Biol. 2015;16:106.
65. Kent WJ. BLAT—the BLAST-like alignment tool. Genome Res. 2002;12:656–64.
66. Stanke M, Schöffmann O, Morgenstern B, Waack S. Gene prediction in eukaryotes with a generalized hidden Markov model that uses hints from external sources. BMC Bioinformatics 2006;7:62.
67. Collart MA, Oliviero S. Preparation of yeast RNA. Curr Protoc Mol Biol. 2001;Chapter 13: Unit 13.12.
68. Bolger AM, Lohse M, Usadel B. Trimmomatic: A flexible trimmer for Illumina Sequence Data. Bioinformatics 2014;30:2114–20.
69. Kim D, Paggi JM, Park C, Bennett C, Salzberg SL. Graph-based genome alignment and genotyping with HISAT2 and HISAT-genotype. Nat Biotechnol. 2019;37:907–15.
70. Li H, Handsaker B, Wysoker A, Fennell T, Ruan J, Homer N, et al. The Sequence alignment/map (SAM) format and SAMtools. Bioinformatics 2009;25:2078–9.
71. Love MI, Huber W, Anders S. Moderated estimation of fold change and dispersion for RNA-seq data with DESeq2. Genome Biol. 2014;15:550.
72. Kolde R. Package 'pheatmap'. 2019. Available from: https://CRAN.R-project.org/package=pheatmap

978 73. Bradford MA. A rapid and sensitive method for the quantitation of microgram quantities of protein
979 utilizing the principle of dye-binding. Anal Biochem. 1976;72: 248–54.
980 74. Michalski A, Damoc E, Lange O, Denisov E, Nolting D, Müller M., et al. Ultra high resolution linear
981 ion trap Orbitrap mass spectrometer (Orbitrap Elite) facilitates top down LC MS/MS and versatile
982 peptide fragmentation modes. Mol Cell Proteomics 2012;11:O111.013698.
983 75. Cox J, Mann M. MaxQuant enables high peptide identification rates, individualized p.p.b.-range
984 mass accuracies and proteome-wide protein quantification. Nat Biotechnol. 2008;26:1367–72.
985 76. Tyanova S, Temu T, Sinitcyn P, Carlson A, Hein MY, Geiger T, et al. The Perseus computational
986 platform for comprehensive analysis of (prote)omics data. Nat Methods 2016;13:731–40.
987 77. Noble SM, Johnson AD. Strains and strategies for large-scale gene deletion studies of the diploid
988 human fungal pathogen *Candida albicans*. Eukaryot Cell 2005;4: 298–309.
989 78. Kosa P, Gavenciakova B, Nosek J. Development of a set of plasmid vectors for genetic
990 manipulations of the pathogenic yeast *Candida parapsilosis*. Gene 2007;396:338–45.
991 79. Gietz RD, Schiestl RH. Transforming yeast with DNA. Methods Mol Cell Biol. 1995;5:255–69.
992 80. Winkler H, Adam G, Mattes E, Schanz M, Hartig A, Ruis H. Co-ordinate control of synthesis of
993 mitochondrial and non-mitochondrial hemoproteins: a binding site for the HAP1 (CYP1) protein in
994 the UAS region of the yeast catalase T gene (*CTT1*). EMBO J. 1988;7:1799–804.
995 81. Edgar RC. MUSCLE: a multiple sequence alignment method with reduced time and space
996 complexity. BMC Bioinformatics 2004;5:113.
997 82. Nguyen LT, Schmidt HA, von Haeseler A, Minh BQ. IQ-TREE: a fast and effective stochastic
998 algorithm for estimating maximum-likelihood phylogenies. Mol Biol Evol. 2015;32:268–74.
999 83. Hoang DT, Chernomor O, von Haeseler A, Minh BQ, Vinh LS. UFBoot2: Improving the Ultrafast
1000 Bootstrap Approximation. Mol Biol Evol. 2018;35:518–22.
1001 84. Gabaldón T. Large-scale assignment of orthology: back to phylogenetics? Genome Biol. 2008;9:
1002 235.
1003 85. Huerta-Cepas J, Gabaldón T. Assigning duplication events to relative temporal scales in genome-
1004 wide studies. Bioinformatics 2011;27:38–45.
1005 86. Perez-Rivero IY, Csordas A, Bai J, Bernal-Llinares M, Hewapathirana S, Kundu DJ, et al. The
1006 PRIDE database and related tools and resources in 2019: improving support for quantification
1007 data. Nucleic Acids Res. 2019;47:D442–50.

87. Katoh K, Standley DM. MAFFT Multiple Sequence Alignment Software Version 7: Improvements in Performance and Usability. Mol Biol Evol. 2013;30:772–80.

88. Kanehisa M, Sato Y, Morishima K. BlastKOALA and GhostKOALA: KEGG tools for functional characterization of genome and metagenome sequences. J Mol Biol. 2016;428:726–31.

89. Kanehisa M, Sato Y. KEGG Mapper for inferring cellular functions from protein sequences. Protein Sci. 2020;29:28–35.

90. Mixão V, Hansen AP, Saus E, Boekhout T, Lass-Florl C, Gabaldón T. Whole-genome sequencing of the opportunistic yeast pathogen *Candida inconspicua* uncovers its hybrid origin. Front Genet. 2019;10:383.

91. Letunic I, Bork P. 20 years of the SMART protein domain annotation resource. Nucleic Acids Res. 2017;46:D493–6.

92. Lin JR, Hu J. SeqNLS: nuclear localization signal prediction based on frequent pattern mining and linear motif scoring. PLoS ONE 2013;8:e76864.

Supporting information captions

S1 Table. RNA-Seq analysis of *C. parapsilosis* cells.

Lists of genes differentially expressed in *C. parapsilosis* CLIB214 cells grown in synthetic media containing 3-hydroxybenzoate, 4-hydroxybenzoate or hydroquinone compared to the cells assimilating galactose (i.e. S3OH vs. SGal, S4OH vs. SGal, SHyd vs. SGal) or 4-hydroxybenzoate (S3OH vs. S4OH, SHyd vs. S4OH). Note that only the genes exhibiting statistically significant $\log_2$ fold change values ($p \leq 0.05$) are shown.

S2 Table. RNA-Seq analysis of *C. parapsilosis* mutants lacking Otf1p or Gtf1p.

Lists of genes differentially expressed in the *C. parapsilosis* mutants Δ*gtf1*/Δ*gtf1* and Δ*otf1*/Δ*otf1* compared to the parental strain CPL2H1 (i.e. Δ*gtf1*/Δ*gtf1* vs. CPL2H1 and Δ*otf1*/Δ*otf1* vs. CPL2H1). The cells were grown in synthetic media (SMix15) containing three hydroxyaromatic carbon sources (i.e. 3-hydroxybenzoate, 4-hydroxybenzoate, and hydroquinone). Note that only the genes exhibiting statistically significant $\log_2$ fold change values ($p \leq 0.05$) are shown.

S3 Table. LC-MS/MS analysis of proteins extracted from *C. parapsilosis* cells.

Lists of proteins identified in the extracts of *C. parapsilosis* CLIB214 cells grown in synthetic media containing 3-hydroxybenzoate (S3OH), 4-hydroxybenzoate (S4OH), hydroquinone (SHyd) or galactose (SGal) as a carbon source. Protein spectra were subjected to label-free quantification (LFQ) and statistically evaluated.

S4 Table. List of synthetic oligonucleotides.

S1 Text. Phylogenetic tree of GTF1 sequences in the Newick format.

S2 Text. Phylogenetic tree of OTF1 sequences in the Newick format.

S1 Fig. Homologs of amidohydrolase family proteins.

Amino acid sequence alignment of conceptual translation of *C. parapsilosis* CANPARB_p44920-A (red shading), short intergenic spacer, and CANPARB_p44910-A (blue shading) with yeast (*C. metapsilosis* (g2237), *T. ciferrii* (KAA8915622.1), *W. sorbophila* (XP_024665283.1), *N. castellii* (XP_003673849.1)) and bacterial (*Pseudomonas aestus* (P308_18355), *Paraburkholderia megapolitana* (SAMN05192543_101920), and *Variovorax* sp. (VAR608DRAFT_1163)) homologs. The alignment was calculated using MAFFT v7.450 (87).

S2 Fig. Expression profiles of *C. parapsilosis* genes coding for metabolic enzymes.
The heatmaps show the expression profiles obtained by the RNA-Seq and LC-MS/MS analyses. The $\log_2$ fold change values obtained by the RNA-Seq analysis (**S1 Table**) are shown on the left panel. Only the genes that are upregulated ($\log_2$ fold change ≥ 2; $p \leq 0.05$) on at least one hydroxyaromatic substrate and code for protein products classified as metabolic enzymes (based on the searches using the BlastKOALA (https://www.kegg.jp/blastkoala/; (88)) and KEGG Mapper tools (https://www.kegg.jp/kegg/tool/map_pathway.html; (89)) are included. Note that the values that are not statistically significant (i.e. $p > 0.05$) are shown in parentheses. The values on the right panel represent $\log_2$ of mean LFQ intensity ratios taken from the LC-MS/MS analysis (**S3 Table**). Note that the LFQ values imputed from a normal distribution were used for proteins that were not identified on all carbon sources (shown in parentheses). Proteins CANPARB_p24940-A and CANPARB_p24960-A, and similarly also CANPARB_p56420-A and CANPARB_p56500-A, have almost identical sequences and therefore could not be distinguished by the LC-MS/MS analysis. Orthologs or best hits (indicated by an asterisk) from the *C. parapsilosis* reference strain CDC317, *C. albicans*, and *S. cerevisiae*, and the KEGG IDs are indicated.

S3 Fig. Acyl-CoA synthetases in *C. parapsilosis*.
(A) The heatmaps show the expression profiles of *C. parapsilosis FAA* genes. The $\log_2$ fold change values obtained by the RNA-Seq analysis (**S1 Table**) are shown on the left panel. Note that the values that are not statistically significant (i.e. $p > 0.05$) are shown in parentheses. The values on the right panel represent $\log_2$ of mean LFQ intensity ratios taken from the LC-MS/MS analysis (**S3 Table**). (B) Phylogenetic relationships of *C. parapsilosis FAA* genes and their homologs in other yeasts. The *CPAR2_200640* gene tree in phylome 498 from PhylomeDB (*Candida inconspicua* genome, described

in (90)) was used as a template to create this figure, which is only shown partially here. Sequences from *C. parapsilosis* (black), *C. albicans* (red), and *S. cerevisiae* (blue) are highlighted with their names. Shadowed rectangles around them indicate, respectively, the spread of species from the *C. parapsilosis sensu lato*, *C. albicans* / *C. dubliniensis* / *C. tropicalis* clade, and *Saccharomyces* / *Nakaseomyces* clade. Colored circles indicate duplication nodes, with different colors indicating the relative age inferred from this duplication (see legend).

S4 Fig. Expression profiles of *C. parapsilosis* genes involved in the biogenesis and metabolism of peroxisomes.

The heatmaps show the expression profiles obtained from the RNA-Seq and LC-MS/MS analyses. The $\log_2$ fold change values obtained by the RNA-Seq analysis (**S1 Table**) are shown on the left panel. Only the genes that are upregulated ($\log_2$ fold change ≥ 2; $p \leq 0.05$) on at least one hydroxyaromatic substrate and code for protein products classified into categories 'peroxisome', 'peroxisomal matrix', 'peroxisomal membrane' or 'peroxisomal importomer complex' (based on the GO subcellular component analysis; http://www.candidagenome.org) are included. Note that the values that are not statistically significant (i.e. $p > 0.05$) are shown in parentheses. The values on the right panel represent $\log_2$ of mean LFQ intensity ratios taken from the LC-MS/MS analysis (**S3 Table**). Orthologs or best hits (indicated by an asterisk) from the *C. parapsilosis* reference strain CDC317, *C. albicans*, and *S. cerevisiae* are shown.

S5 Fig. Amino acid sequence alignments of Otf1p and Gtf1p orthologs.

(A) Amino acid sequence alignment of *C. parapsilosis* Otf1p with the counterparts from *C. metapsilosis* (CMET_1974), *C. orthopsilosis* (CORT0C05870), *C. albicans* (ZCF10), *C. tropicalis* (CTRG_01734), *Scheffersomyces stipitis* (PICST_62477), and *Spathaspora passalidarum* (SPAPADRAFT_137814). (B) Amino acid sequence alignment of *C. parapsilosis* Gtf1p with the counterparts from *C. metapsilosis* (CMET_1081), *S. passalidarum* (SPAPADRAFT_53773), *Debaryomyces hansenii* (DEHA2C00946g), and *S. stipitis* (PICST_57167 and PICST_65252). The alignments were calculated using MAFFT v7.450 (87). The GAL4-like domain (red shading) and fungal specific transcription factor domain (blue shading) were predicted using SMART 8.0 (91). Nuclear localisation signal (NLS, shown in magenta) was identified using SeqNLS (92).

S6 Fig. Downregulated genes in *C. parapsilosis* mutants lacking Otf1p or Gtf1p.

The heatmap shows the genes downregulated (log_2 fold change ≤ -2; p ≤ 0.05; **S2 Table**) in the mutants Δ*gtf1*/Δ*gtf1* and Δ*otf1*/Δ*otf1* compared to the parental strain CPL2H1 (Δ*gtf1*/Δ*gtf1* vs. CPL2H1 and Δ*otf1*/Δ*otf1* vs. CPL2H1). The cells were grown in an SMix15 medium containing three hydroxyaromatic carbon sources (i.e. 3-hydroxybenzoate, 4-hydroxybenzoate, and hydroquinone). Note that the values that are not statistically significant (i.e. p > 0.05) are shown in parentheses. Orthologs or best hits (indicated by an asterisk) from *C. parapsilosis* CDC317, *C. albicans,* and *S. cerevisiae,* and KEGG IDs are indicated.

S7 Fig. Putative binding sites for Otf1p and Gtf1p in the promoters of 3-OAP and GP genes.

The occurrence of putative Otf1p (A; shown as blue triangles) and Gtf1p (B; blue rectangles) binding sites in the upstream regions of the genes encoding the components of the 3-OAP and GP, respectively. Putative Mig1p-binding sites (red triangles) and the positions of probes used in the EMSA experiments (black rectangles) are also depicted.

S8 Fig. Predicted Otf1p and Gtf1p binding motifs.

(A) Otf1p binding motif. (B) Gtf1p binding motif. The sequence logos were derived from predicted binding sites identified in the promoter sequences shown in **S7 Fig**.

S9 Fig. Consumption of hydroxyaromatic substrates by *C. parapsilosis* cells.

C. parapsilosis CLIB214 cells grown in the synthetic media containing a hydroxyaromatic substrate as a sole carbon source at 28 °C till OD_{600} ~ 1. Substrate consumption was inferred from the absorption spectra (200-350 nm) measured in the media of three parallel cultures (shown in red, blue, and green) after cultivation (t = 17.5, 25.5, and 16 hours for 3-hydroxybenzoate, 4-hydroxybenzoate, and hydroquinone, respectively) as well as in the control medium. Each measurement was performed in three technical replicates. The samples were diluted 2-, 20-, and 5-fold prior analysis of 3-hydroxybenzoate, 4-hydroxybenzoate, and hydroquinone consumption, respectively.

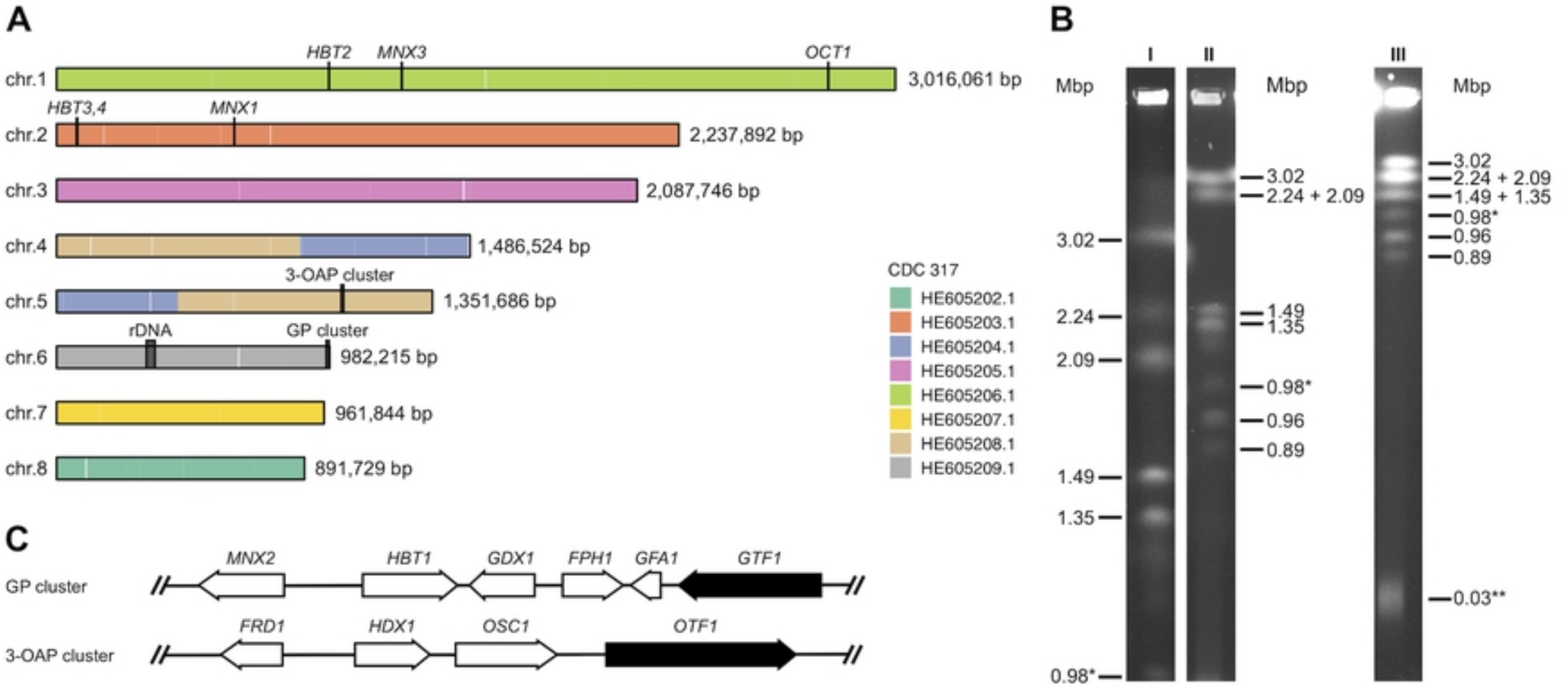
A
HBT2
MNX3
OCT1
chr.1
3,016,061 bp
HBT3,4
MNX1
chr.2
2,237,892 bp
chr.3
2,087,746 bp
chr.4
1,486,524 bp
3-OAP cluster
chr.5
1,351,686 bp
rDNA
GP cluster
chr.6
982,215 bp
chr.7
961,844 bp
chr.8
891,729 bp
CDC 317
HE605202.1
HE605203.1
HE605204.1
HE605205.1
HE605206.1
HE605207.1
HE605208.1
HE605209.1
B
I
II
III
Mbp
Mbp
Mbp
3.02
2.24
2.09
1.49
1.35
0.98*
3.02
2.24 + 2.09
1.49
1.35
0.98*
0.96
0.89
3.02
2.24 + 2.09
1.49 + 1.35
0.98*
0.96
0.89
0.03**
C
GP cluster
MNX2
HBT1
GDX1
FPH1
GFA1
GTF1
3-OAP cluster
FRD1
HDX1
OSC1
OTF1

Fig 1

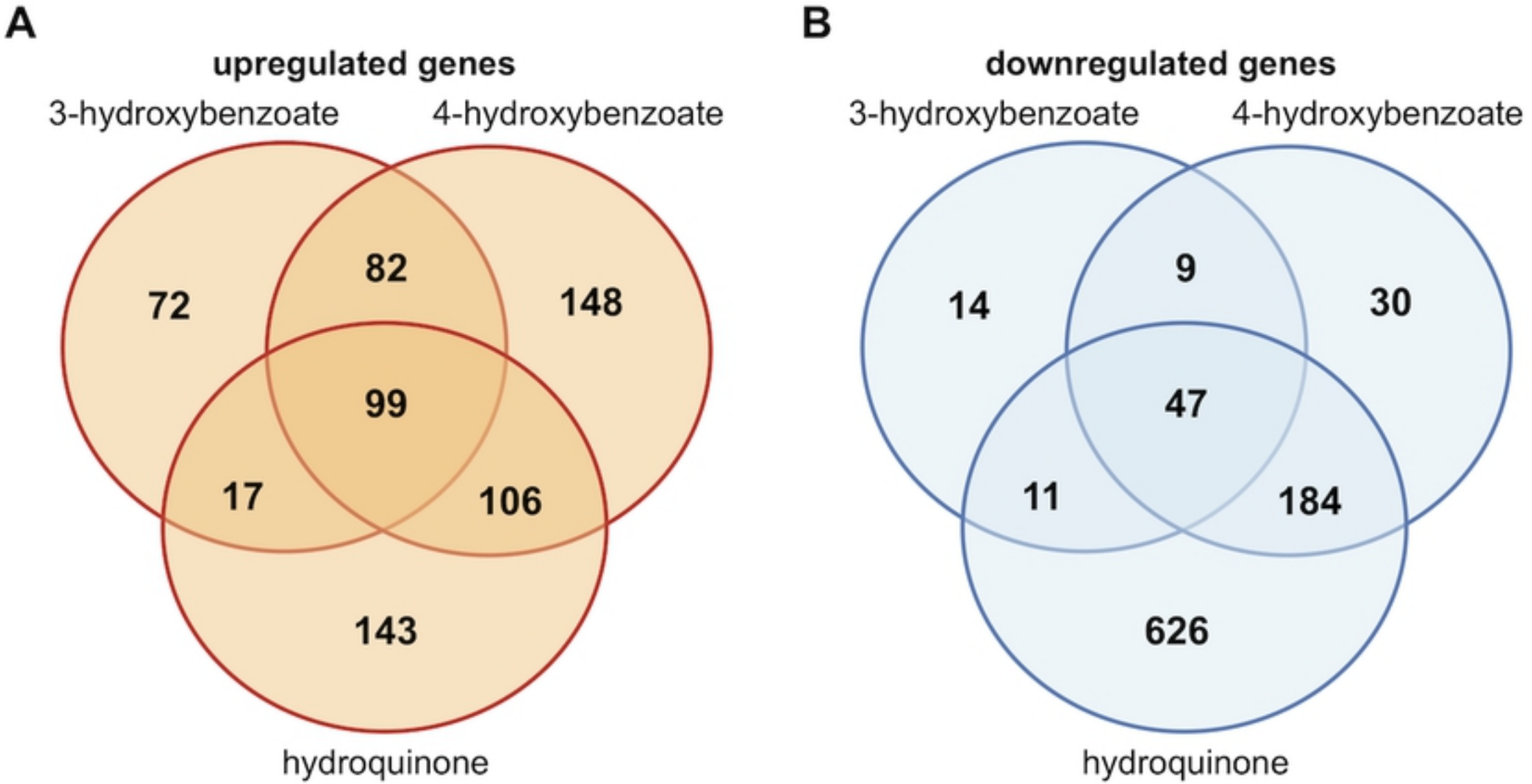
A
upregulated genes
3-hydroxybenzoate
4-hydroxybenzoate
72
82
148
99
17
106
143
hydroquinone
B
downregulated genes
3-hydroxybenzoate
4-hydroxybenzoate
14
9
30
47
11
184
626
hydroquinone

Fig 2

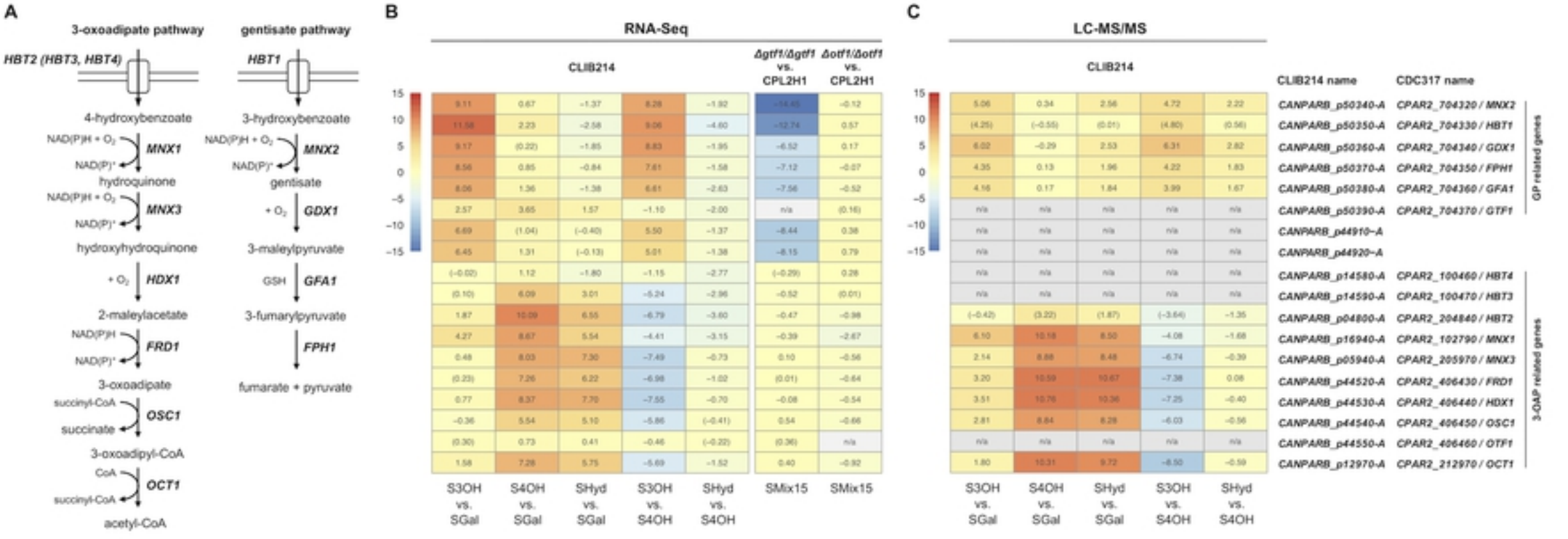
A
3-oxoadipate pathway
gentisate pathway
HBT2 (HBT3, HBT4)
HBT1
4-hydroxybenzoate
3-hydroxybenzoate
NAD(P)H + O2
NAD(P)+
MNX1
MNX2
hydroquinone
gentisate
MNX3
+ O2
GDX1
hydroxyhydroquinone
3-maleylpyruvate
HDX1
GSH
GFA1
2-maleylacetate
3-fumarylpyruvate
NAD(P)H
FRD1
FPH1
3-oxoadipate
fumarate + pyruvate
succinyl-CoA
OSC1
succinate
3-oxoadipyl-CoA
CoA
OCT1
succinyl-CoA
acetyl-CoA
B
RNA-Seq
CLIB214
Δgtf1/Δgtf1 vs. CPL2H1
Δotf1/Δotf1 vs. CPL2H1
15
10
5
0
−5
−10
−15
S3OH vs. SGal
S4OH vs. SGal
SHyd vs. SGal
S3OH vs. S4OH
SHyd vs. S4OH
SMix15
SMix15
C
LC-MS/MS
CLIB214
S3OH vs. SGal
S4OH vs. SGal
SHyd vs. SGal
S3OH vs. S4OH
SHyd vs. S4OH
CLIB214 name
CDC317 name
CANPARB_p50340-A
CPAR2_704320 / MNX2
CANPARB_p50350-A
CPAR2_704330 / HBT1
CANPARB_p50360-A
CPAR2_704340 / GDX1
CANPARB_p50370-A
CPAR2_704350 / FPH1
CANPARB_p50380-A
CPAR2_704360 / GFA1
CANPARB_p50390-A
CPAR2_704370 / GTF1
GP related genes
CANPARB_p44910-A
CANPARB_p44920-A
CANPARB_p14580-A
CPAR2_100460 / HBT4
CANPARB_p14590-A
CPAR2_100470 / HBT3
CANPARB_p04800-A
CPAR2_204840 / HBT2
CANPARB_p16940-A
CPAR2_102790 / MNX1
CANPARB_p05940-A
CPAR2_205970 / MNX3
CANPARB_p44520-A
CPAR2_406430 / FRD1
CANPARB_p44530-A
CPAR2_406440 / HDX1
CANPARB_p44540-A
CPAR2_406450 / OSC1
CANPARB_p44550-A
CPAR2_406460 / OTF1
CANPARB_p12970-A
CPAR2_212970 / OCT1
3-OAP related genes

Fig 3

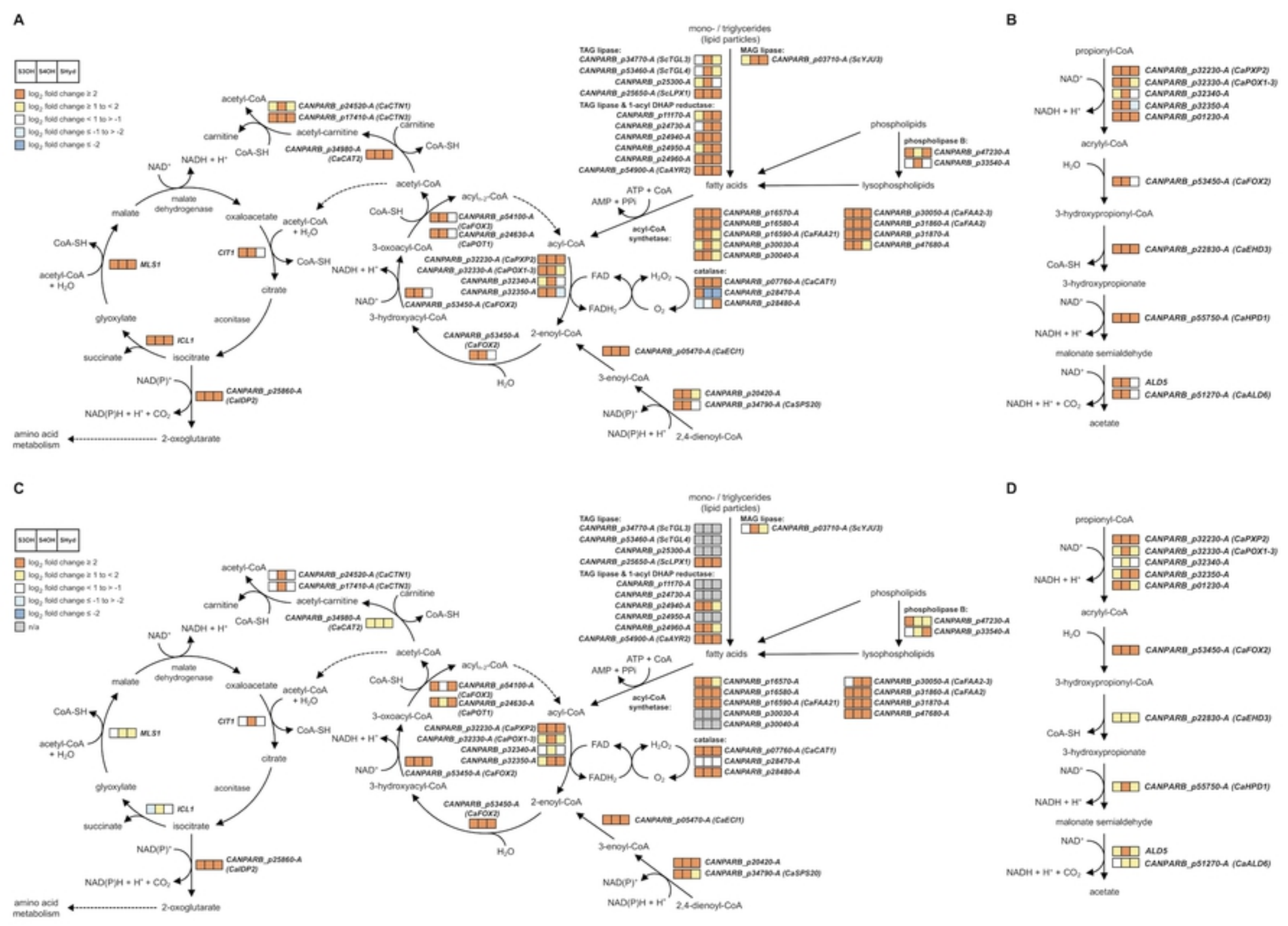
A
B
C
D
S3OH
S4OH
SHyd
log2 fold change ≥ 2
log2 fold change ≥ 1 to < 2
log2 fold change < 1 to > -1
log2 fold change ≤ -1 to > -2
log2 fold change ≤ -2
n/a
mono- / triglycerides
(lipid particles)
TAG lipase:
CANPARB_p34770-A (ScTGL3)
CANPARB_p53460-A (ScTGL4)
CANPARB_p25300-A
CANPARB_p25650-A (ScLPX1)
TAG lipase & 1-acyl DHAP reductase:
CANPARB_p11770-A
CANPARB_p24730-A
CANPARB_p24940-A
CANPARB_p24950-A
CANPARB_p24960-A
CANPARB_p54900-A (CaAYR2)
MAG lipase:
CANPARB_p03710-A (ScYJU3)
phospholipids
phospholipase B:
CANPARB_p47230-A
CANPARB_p33540-A
fatty acids
lysophospholipids
ATP + CoA
AMP + PPi
acyl-CoA synthetase:
CANPARB_p16570-A
CANPARB_p16580-A
CANPARB_p16590-A (CaFAA21)
CANPARB_p30030-A
CANPARB_p30040-A
CANPARB_p30050-A (CaFAA2-3)
CANPARB_p31860-A (CaFAA2)
CANPARB_p31870-A
CANPARB_p47680-A
catalase:
CANPARB_p07760-A (CaCAT1)
CANPARB_p28470-A
CANPARB_p28480-A
acetyl-CoA
carnitine
acetyl-carnitine
CoA-SH
CANPARB_p24520-A (CaCTN1)
CANPARB_p17410-A (CaCTN3)
CANPARB_p34980-A (CaCAT2)
NAD+
NADH + H+
malate
malate dehydrogenase
oxaloacetate
acetyl-CoA + H2O
CIT1
citrate
aconitase
isocitrate
MLS1
glyoxylate
ICL1
succinate
NAD(P)+
NAD(P)H + H+ + CO2
CANPARB_p25860-A (CaIDP2)
amino acid metabolism
2-oxoglutarate
acyl(n-2)-CoA
CANPARB_p54100-A (CaFOX3)
CANPARB_p24630-A (CaPOT1)
3-oxoacyl-CoA
CANPARB_p32230-A (CaPXP2)
CANPARB_p32330-A (CaPOX1-3)
CANPARB_p32340-A
CANPARB_p32350-A
CANPARB_p53450-A (CaFOX2)
3-hydroxyacyl-CoA
acyl-CoA
FAD
FADH2
H2O2
O2
2-enoyl-CoA
CANPARB_p05470-A (CaECI1)
3-enoyl-CoA
CANPARB_p20420-A
CANPARB_p34790-A (CaSPS20)
NAD(P)+
NAD(P)H + H+
2,4-dienoyl-CoA
propionyl-CoA
acrylyl-CoA
3-hydroxypropionyl-CoA
3-hydroxypropionate
malonate semialdehyde
CANPARB_p01230-A
CANPARB_p22830-A (CaEHD3)
CANPARB_p55750-A (CaHPD1)
ALD5
CANPARB_p51270-A (CaALD6)
acetate

Fig 4

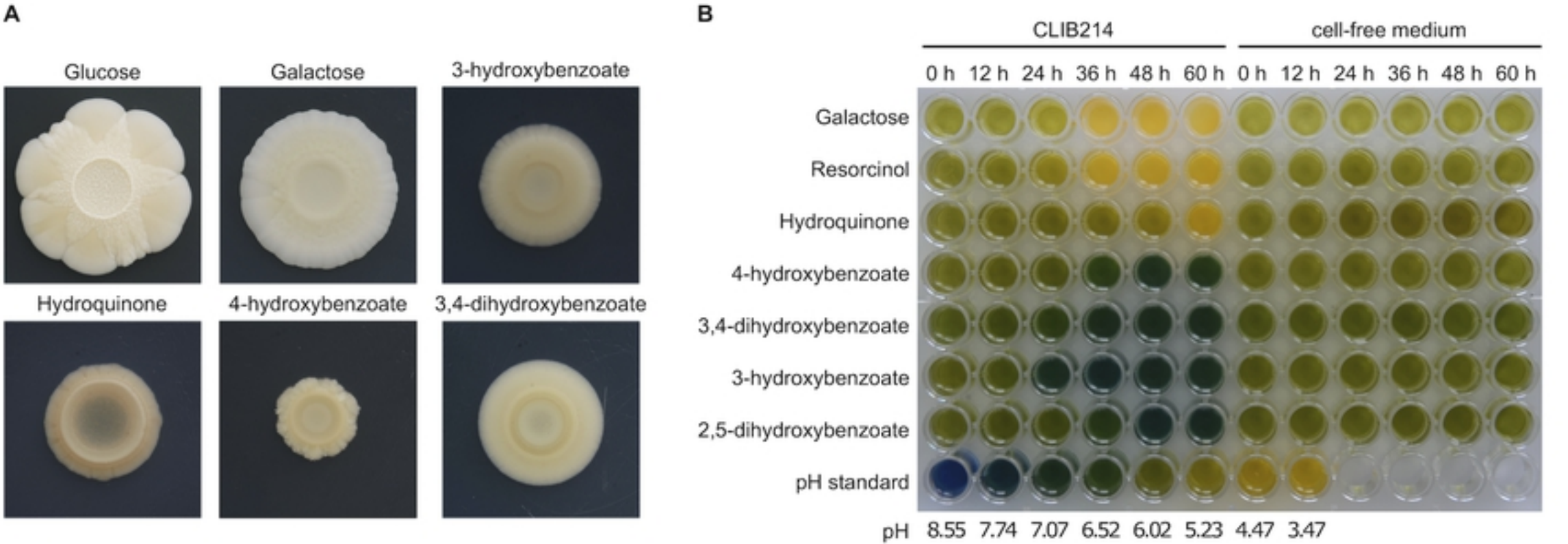
A
Glucose
Galactose
3-hydroxybenzoate
Hydroquinone
4-hydroxybenzoate
3,4-dihydroxybenzoate
B
CLIB214
cell-free medium
0 h 12 h 24 h 36 h 48 h 60 h 0 h 12 h 24 h 36 h 48 h 60 h
Galactose
Resorcinol
Hydroquinone
4-hydroxybenzoate
3,4-dihydroxybenzoate
3-hydroxybenzoate
2,5-dihydroxybenzoate
pH standard
pH 8.55 7.74 7.07 6.52 6.02 5.23 4.47 3.47

Fig 6

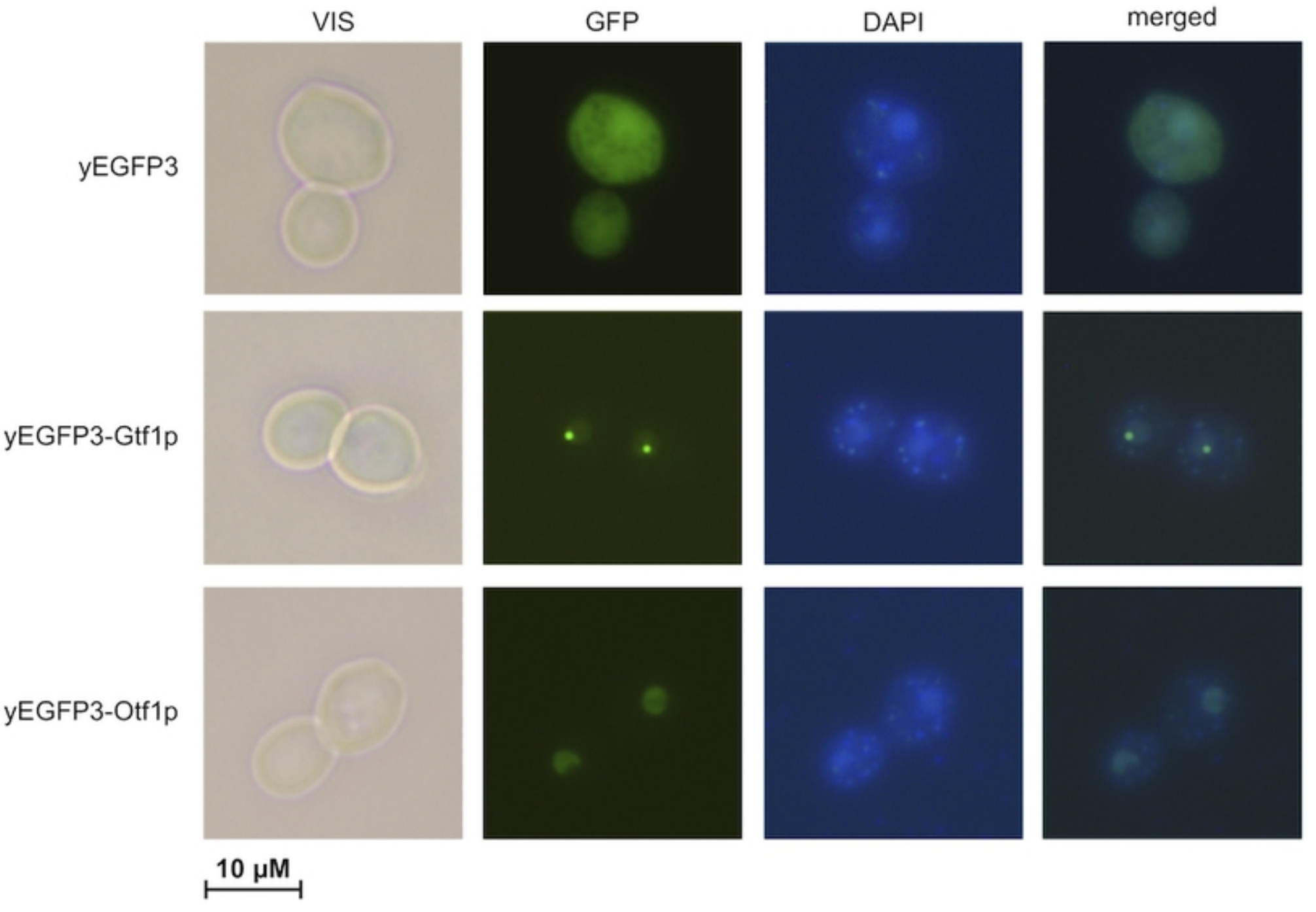

Fig 7

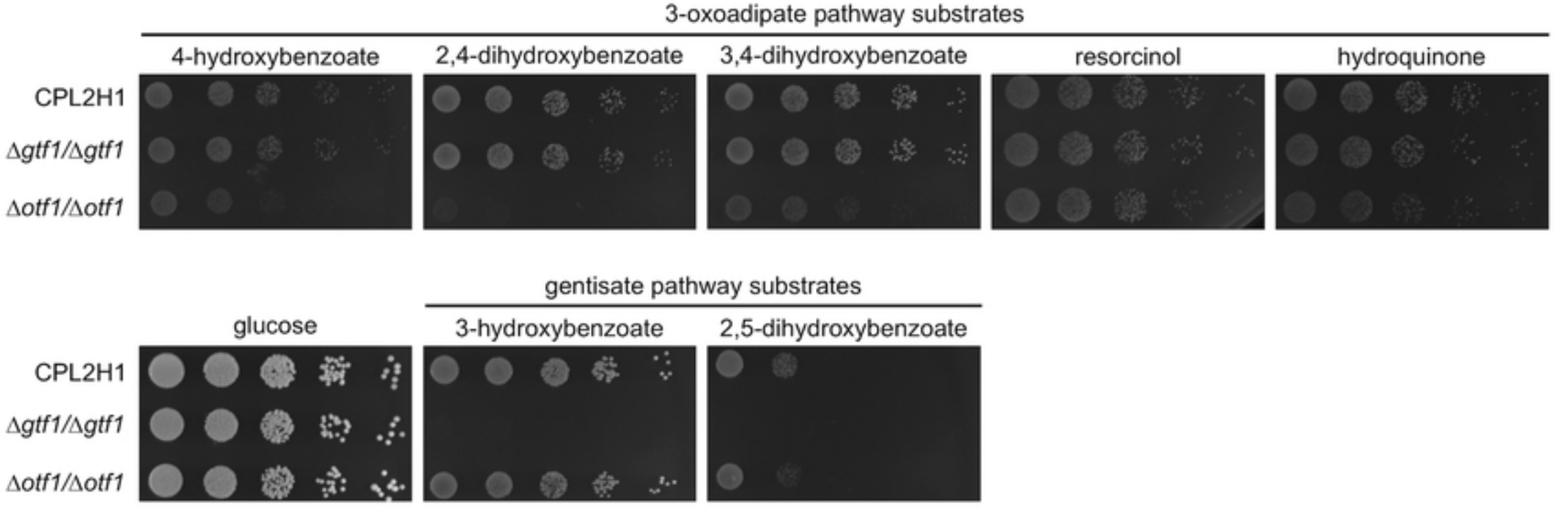
3-oxoadipate pathway substrates
4-hydroxybenzoate
2,4-dihydroxybenzoate
3,4-dihydroxybenzoate
resorcinol
hydroquinone
CPL2H1
Δgtf1/Δgtf1
Δotf1/Δotf1
gentisate pathway substrates
glucose
3-hydroxybenzoate
2,5-dihydroxybenzoate
CPL2H1
Δgtf1/Δgtf1
Δotf1/Δotf1

Fig 8

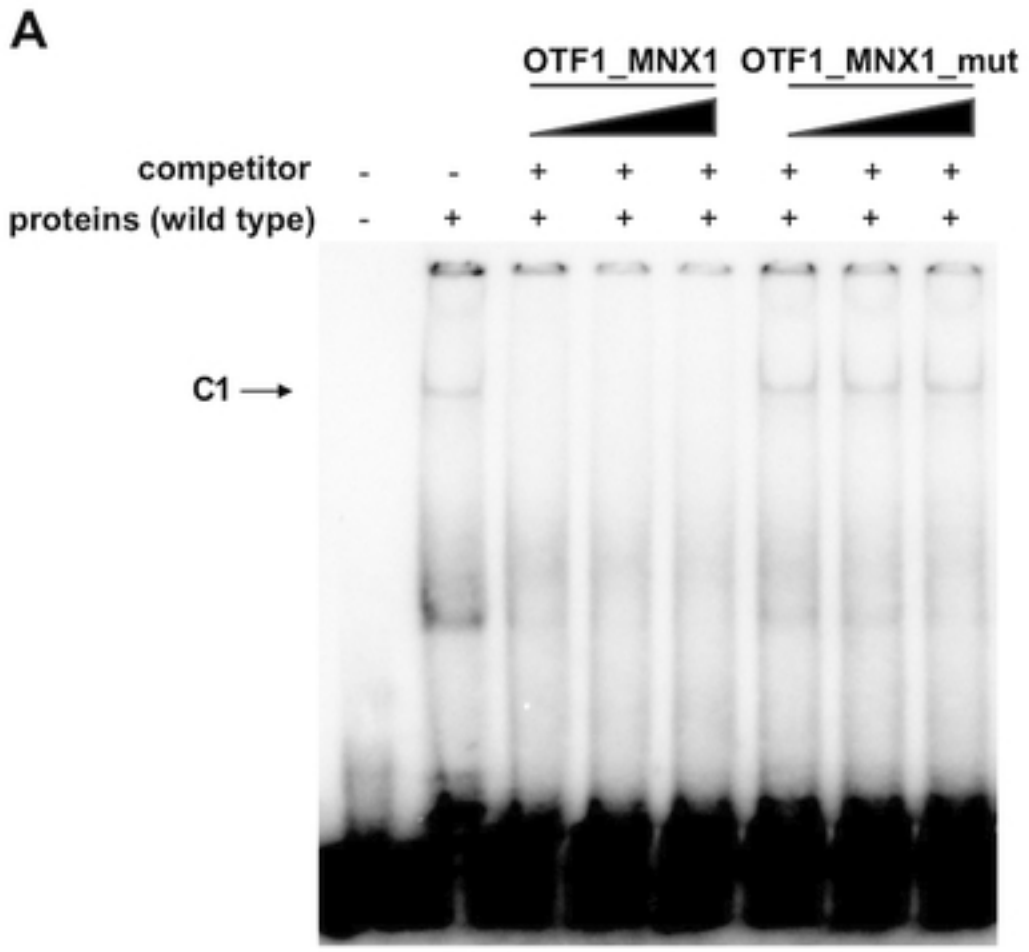

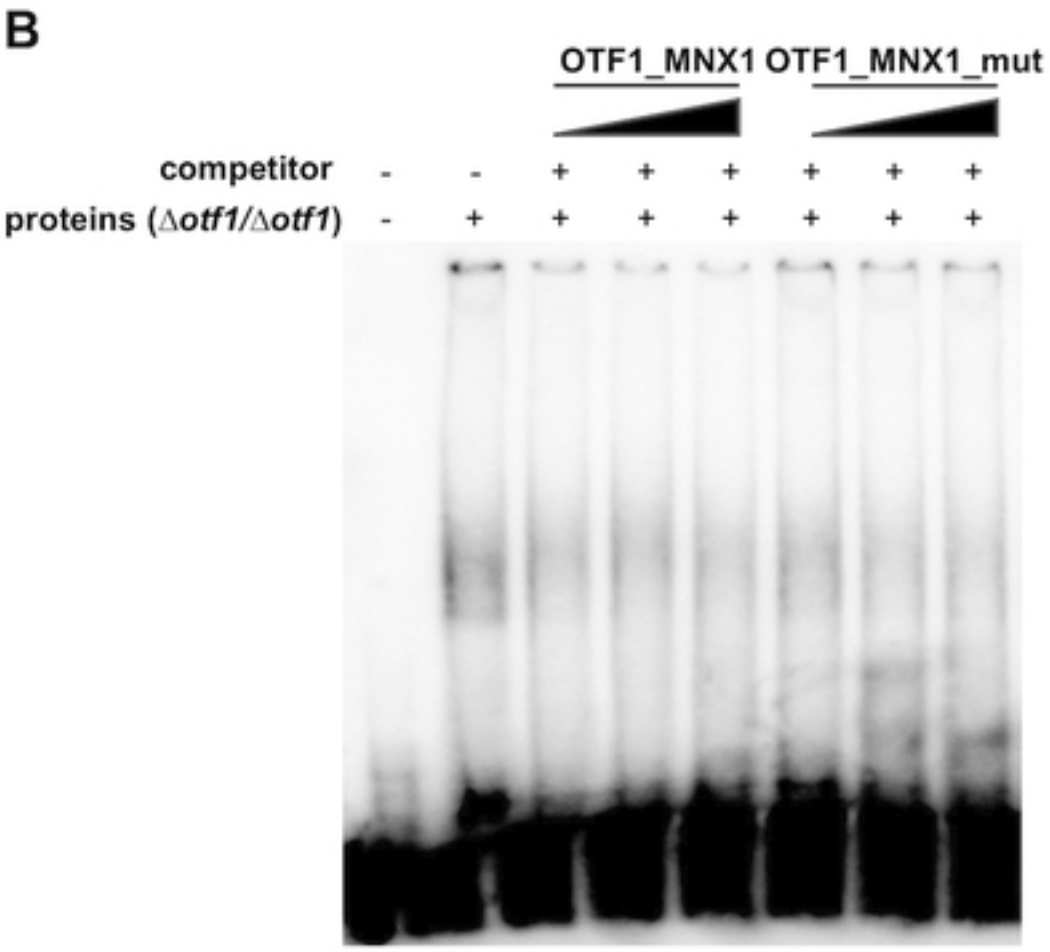

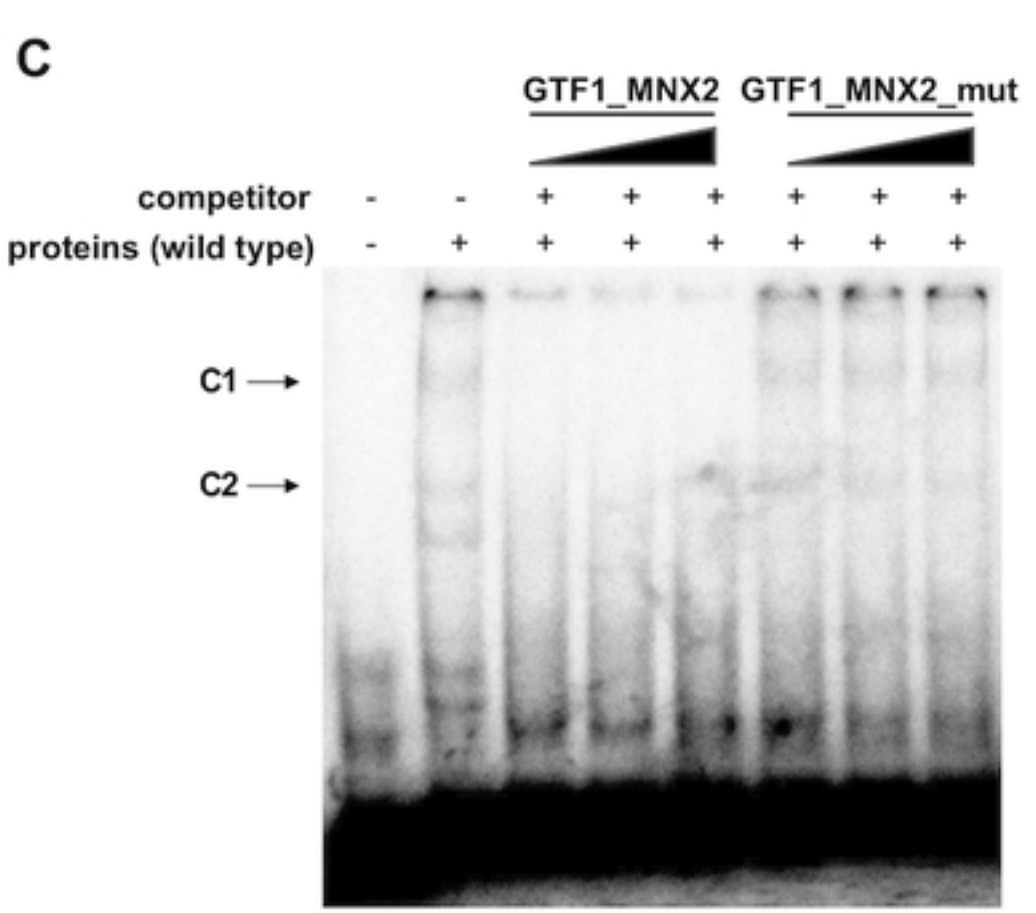

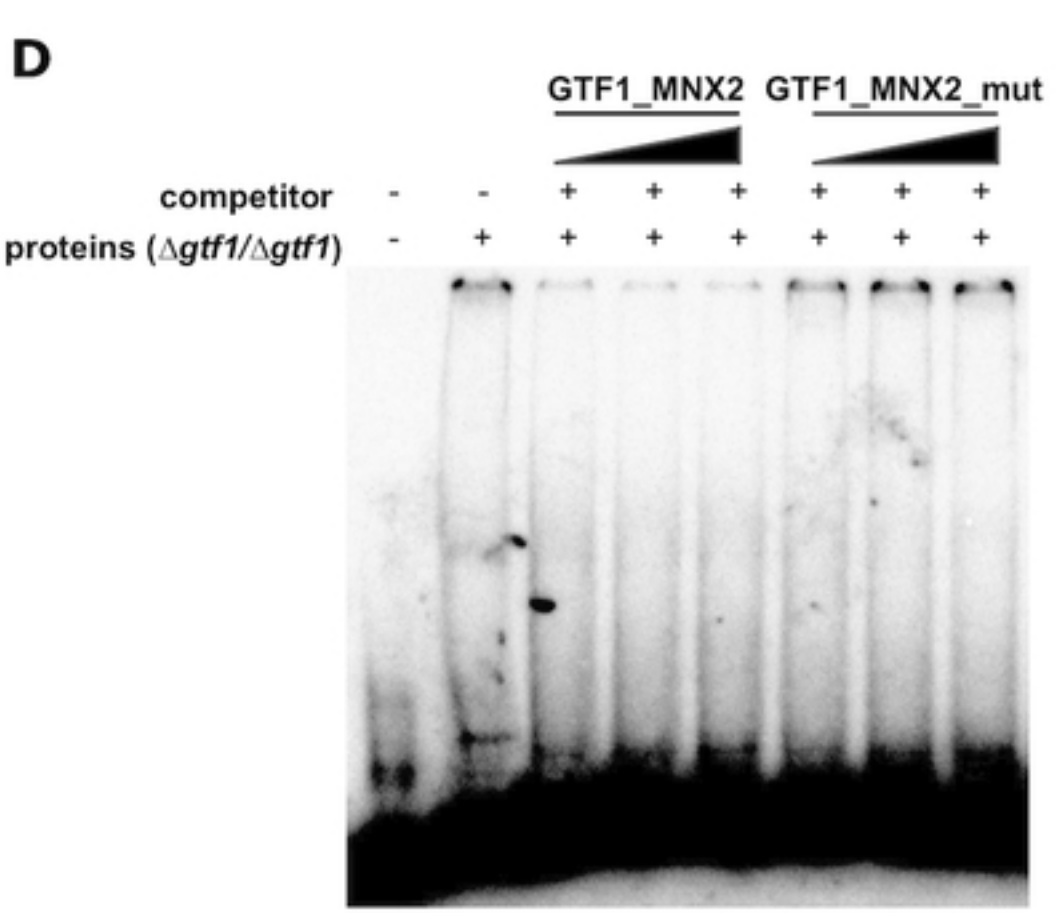

Fig 9

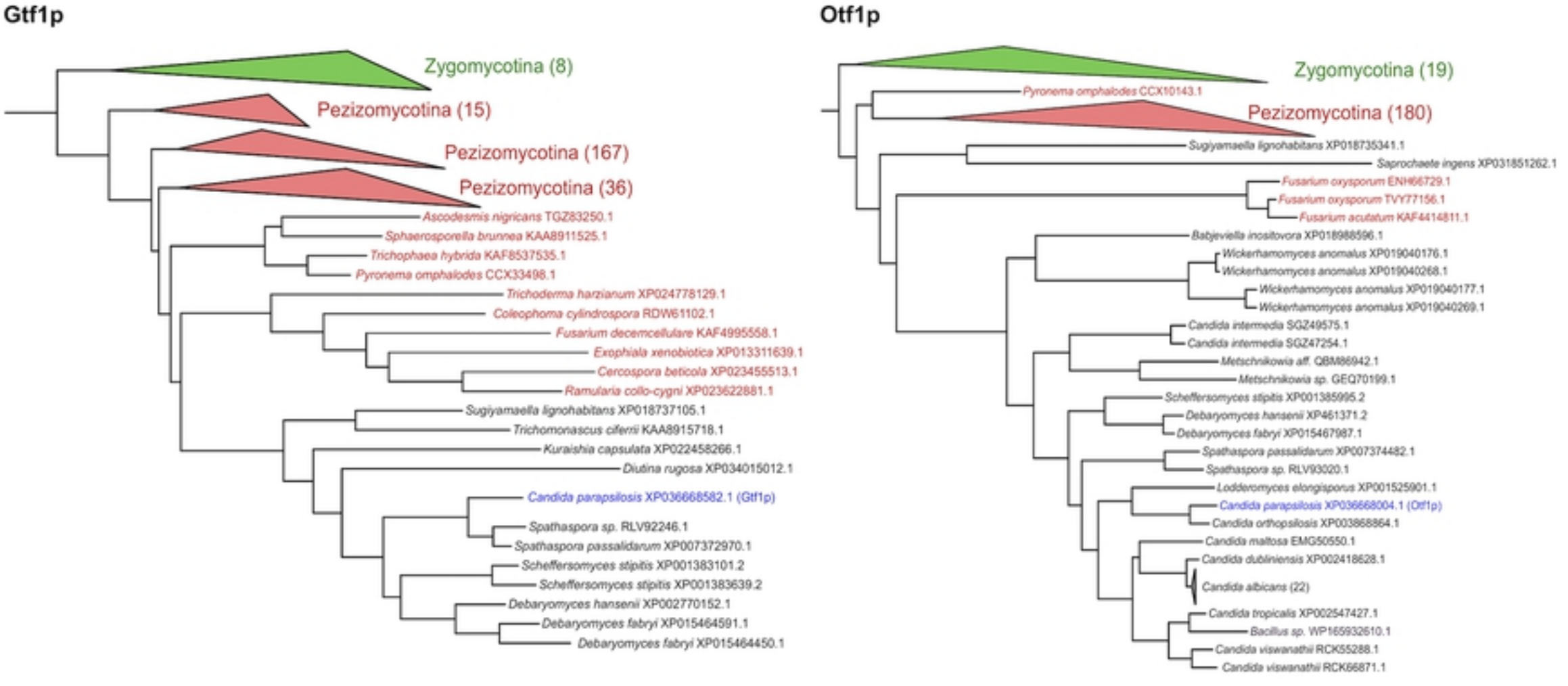
Gtf1p
Zygomycotina (8)
Pezizomycotina (15)
Pezizomycotina (167)
Pezizomycotina (36)
Ascodesmis nigricans TGZ83250.1
Sphaerosporella brunnea KAA8911525.1
Trichophaea hybrida KAF8537535.1
Pyronema omphalodes CCX33498.1
Trichoderma harzianum XP024778129.1
Colecphoma cylindrospora RDW61102.1
Fusarium decemcellulare KAF4995558.1
Exophiala xenobiotica XP013311639.1
Cercospora beticola XP023455513.1
Ramularia collo-cygni XP023622881.1
Sugiyamaella lignohabitans XP018737105.1
Trichomonascus ciferrii KAA8915718.1
Kuraishia capsulata XP022458266.1
Diutina rugosa XP034015012.1
Candida parapsilosis XP036668582.1 (Gtf1p)
Spathaspora sp. RLV92246.1
Spathaspora passalidarum XP007372970.1
Scheffersomyces stipitis XP001383101.2
Scheffersomyces stipitis XP001383639.2
Debaryomyces hansenii XP002770152.1
Debaryomyces fabryi XP015464591.1
Debaryomyces fabryi XP015464450.1
Otf1p
Zygomycotina (19)
Pyronema omphalodes CCX10143.1
Pezizomycotina (180)
Sugiyamaella lignohabitans XP018735341.1
Saprochaete ingens XP031851262.1
Fusarium oxysporum ENH66729.1
Fusarium oxysporum TVY77156.1
Fusarium acutatum KAF4414811.1
Babjeviella inositovora XP018988596.1
Wickerhamomyces anomalus XP019040176.1
Wickerhamomyces anomalus XP019040268.1
Wickerhamomyces anomalus XP019040177.1
Wickerhamomyces anomalus XP019040269.1
Candida intermedia SGZ49575.1
Candida intermedia SGZ47254.1
Metschnikowia aff. QBM86942.1
Metschnikowia sp. GEQ70199.1
Scheffersomyces stipitis XP001385995.2
Debaryomyces hansenii XP461371.2
Debaryomyces fabryi XP015467987.1
Spathaspora passalidarum XP007374482.1
Spathaspora sp. RLV93020.1
Lodderomyces elongisporus XP001525901.1
Candida parapsilosis XP036668004.1 (Otf1p)
Candida orthopsilosis XP003868864.1
Candida maltosa EMG50550.1
Candida dubliniensis XP002418628.1
Candida albicans (22)
Candida tropicalis XP002547427.1
Bacillus sp. WP165932610.1
Candida viswanathii RCK55288.1
Candida viswanathii RCK66871.1

Fig 10

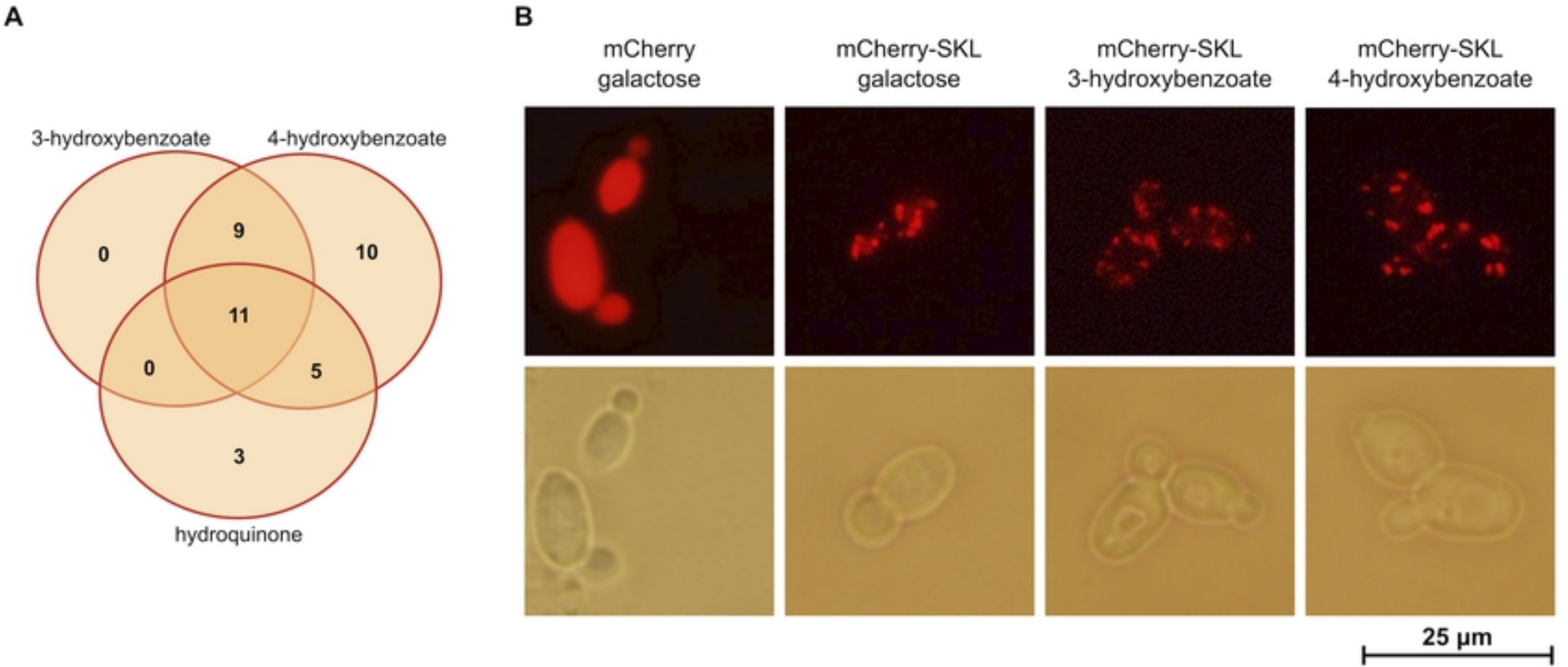
A
3-hydroxybenzoate
4-hydroxybenzoate
hydroquinone
0
9
10
11
0
5
3
B
mCherry
galactose
mCherry-SKL
galactose
mCherry-SKL
3-hydroxybenzoate
mCherry-SKL
4-hydroxybenzoate
25 µm

Fig 5